SOUTHEASTERN

GEOLOGY

This journal welcomes original papers on all phases of geology, geophysics, and geochemistry as related to the Southeast. Transmit manuscripts to S. DUNCAN HERON, JR., BOX 6665, COLLEGE STATION, DURHAM, NORTH CAROLINA. Please observe the following:

(1) Type the manuscript with double space lines and submit in duplicate.
(2) Cite references and prepare bibliographic lists in accordance with the method found within the pages of this journal.
(3) Submit line drawings and complex tables as finished copy.
(4) Make certain that all photographs are sharp, clear, and of good contrast.
(5) Stratigraphic terminology should abide by the Code of Stratigraphic Nomenclature (AAPG, v. 45, 1961).

Proofs will not be sent authors unless a request to this effect accompanies the manuscript.

Reprints must be ordered prior to publication. Prices are available upon request.

* * * * * *

Subscriptions to Southeastern Geology are $5.00 per volume. Inquiries should be addressed to WM. J. FURBISH, BUSINESS AND CIRCULATION MANAGER, BOX 6665, COLLEGE STATION, DURHAM NORTH CAROLINA. Make check payable to Southeastern Geology.

SOUTHEASTERN GEOLOGY

Table of Contents

Vol. 15, No. 1

1973

RELATIONSHIP BETWEEN MICROSCOPIC FABRIC AND MESOSCOPIC STRUCTURE IN A DEFORMED SUPRACRUSTAL ASSEMBLAGE, WEST-CENTRAL PIEDMONT OF VIRGINIA

By

S. G. Khoury
and
M. Lofti Abdel-Khalek*
Department of Earth and Planetary Sciences
University of Pittsburgh
Pittsburgh, Pennsylvania 15213

ABSTRACT

The rocks in the vicinity of Otter River, in the west-central Piedmont of Virginia, represent a metamorphosed supracrustal assemblage which has been affected by multiphase deformation.

A textural and petrofabric study was undertaken to compare the effect of each phase of deformation on the various mineral constituents. The hornblende subfabric and the mesoscopic structures were found to be generally homotactic, although multiple deformation tends to obscure this relationship. The orientation of the mica is controlled by the prominent foliation $S_1 // S_2$ and to a lesser extent by the late cleavage S_3. The quartz subfabric is variable in the different rock groups. Patterns of (0001) axes and poles to deformation lamellae in quartz were used to determine the orientation of the three principal axes of stress σ_1, σ_2, and σ_3 during each of the last two periods of deformation.

A correlation with the mesoscopic and microscopic fabrics across the Catoctin Mountain-Blue Ridge anticlinorium suggests that in Central Virginia the portion of the Inner-Piedmont and Blue-Ridge that extends from Bedford to the north of Lovingston, Virginia, had a uniform structural evolution.

INTRODUCTION

The rocks in the vicinity of Otter River, in the west-central Piedmont of Virginia (Figure 1), have been affected by multiphase deformation during a period of crustal disturbance. The major rock types in the area grade from chloritoid-graphite phyllites in the southeast, to hornblende gneisses in the northwest. This gradual transition reflects a continuous change in metamorphic grade from lower greenschist

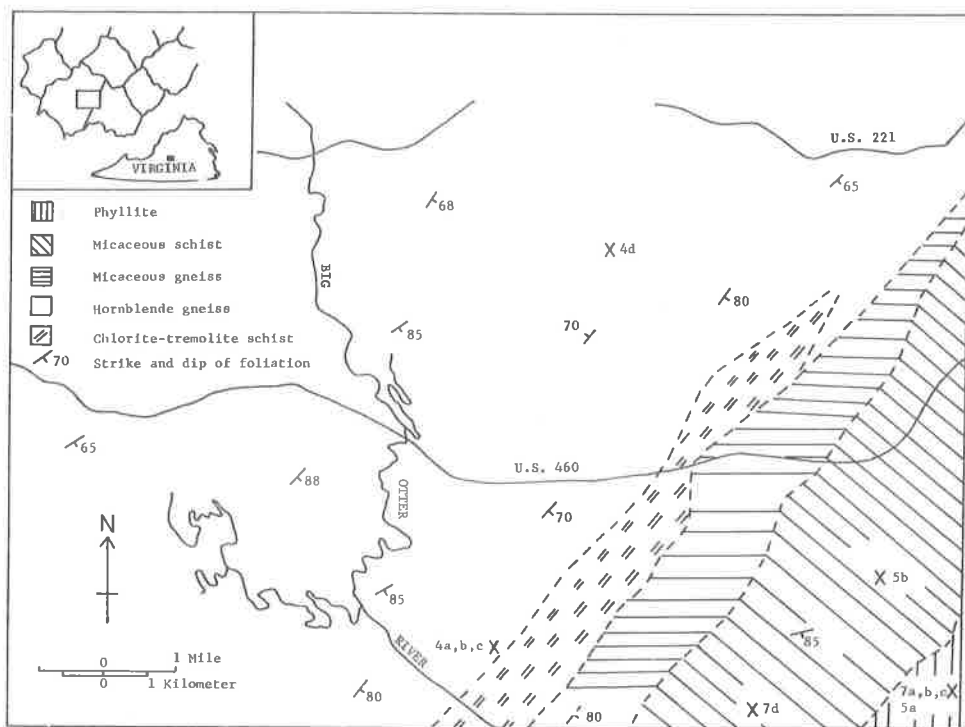*Present Address: Geology Department, Cairo University, A.R.E.

1

Figure 1. Generalized geologic map of the Otter River area showing the relative position of the samples used in the petrofabric analysis.

facies to upper amphibolite facies and represents the progressive metamorphism of a supracrustal assemblage (Figure 1 and Abdel-Khalek and Khoury, 1971).

The most prominent structural feature of the area is a well-developed subvertical foliation parallel to the lithologic layering. At several localities the foliation and the lithologic layering were found to parallel metasedimentary bands in which a relict sedimentary bedding, S_0, can still be recognized. Isoclinal folds F_1 are widely distributed in the hornblende gneiss. The associated axial plane foliation S_1 is essentially parallel to the layering. The mineral lineation L_1 parallels the axes of the isoclines. Asymmetrical flexural folds, F_2, have changed the disposition of the original layering, S_0, and conformable foliation, S_1, from subhorizontal to steep or subvertical, striking northeast-southwest. A steeply-dipping cleavage, S_2, and a subhorizontal crenulation lineation, L_2, are closely related to the development of these folds. Open concentric flexural folds, F_3, deform but do not appreciably alter the general orientation of the pre-existing foliation and cleavage. These folds are associated with a strain slip cleavage, S_3, cross-
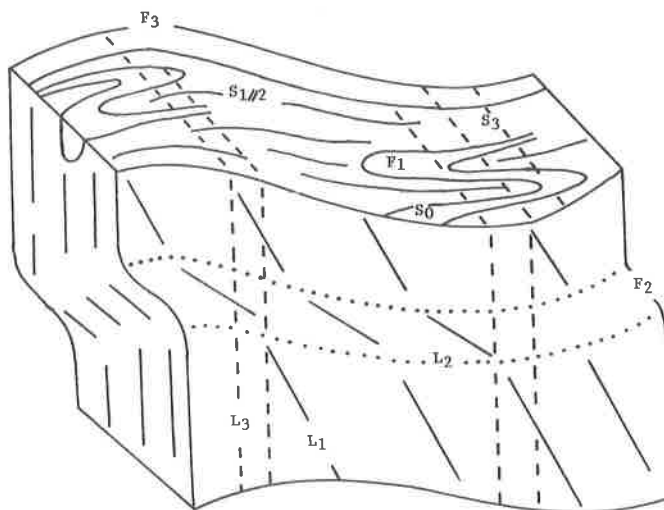
2

Figure 2. Hypothetical block diagram showing
the spatial relationship between the various
structural elements described in the text.

cutting the pre-existing surfaces at a large angle. A steeply plunging
lineation, L_3, is parallel to the fold axes. The geometric relationship
between the various structural elements is shown diagrammatically in
Figure 2. (See also Abdel-Khalek and Khoury, 1971, Figure 7).

Acknowledgments

This paper has benefited from the critical reviews and the sug-
gestions made by D. E. Dunn, University of North Carolina, E. G.
Lidiak, University of Pittsburgh, R. D. Hatcher, Jr. and V. S. Griffin,
Jr., Clemson University, and J. F. Conley, Virginia Division of Mine-
ral Resources.

STRUCTURAL ANALYSIS

The contoured projection of foliation planes shows a single elon-
gate maximum defining a statistical foliation oriented N 54° E, dipping
78° SE. The great circle, partial π-girdle, has a π-axis oriented
S 48° E, plunging 78° SE. This π-axis, which represents a statistical
axis of folding, falls within the domain of the L_3 lineation. There is
also a statistical tendency toward a partial sub-vertical π-girdle orient-
ed N 34° W 85° SW. The corresponding pole falls within the domain of
the L_2 lineation (Abdel-Khalek and Khoury, 1971, Figure 7).

3

MICROFABRIC ANALYSIS

The subfabrics of hornblende, from the hornblende gneiss, and of mica and quartz, from the phyllite and mica schist (Figure 1) were examined. The advantage of simultaneously observing the subfabric of hornblende, mica and quartz is in the possible comparison of the behavior of various minerals which have had a common deformational history. The subfabric diagrams are presented with the plane of the thin section in the plane of the paper, and the strike of the regional foliation coinciding with its field orientation. The appropriate geographic coordinates and the mesoscopic fabric elements are plotted on each diagram to provide a direct visual comparison between the mesoscopic elements and the mineral subfabrics.

The Hornblende Subfabric

Several thin sections were cut from a foliated hornblende gneiss showing well-developed isoclinal folds. A strong mineral lineation (L_1) parallels the axes of the isoclines. This mineral alignment is enhanced by the weathering of the exposed foliation plane. Hornblende grains, a fraction to 1 mm. long, form stringers stretched parallel to $b_1 = B$. Therefore, in hand specimen, the rock is considered to be a good hornblende - B - tectonite.

Orientation Procedure - By measuring the indicatrix, or merely the position of Y and that of a cleavage plane, all other important crystallographic directions for the study of the hornblende fabric can be reconstructed (Briegleb, 1966, p. 311-312). Although theoretically sound, this method depends on the accurate determination of the vertical position of a cleavage plane. For crystal sections inclined at a large angle to (001) this may not always be easy to define (Turner, 1942; Hess, 1949, p. 630). In these cases, the c-axes obtained by the intersection of (010) and (110) have the largest degree of error (Figure 3a and Schwerdtner, 1964, p. 1215).

The angle between c and z, obtained from sections parallel to (001), was found to be 17° (Figure 3b). For common hornblende, this angle was estimated to be between 15° and 25° (Winchell and Winchell, 1951; Tröger, 1959, p. 68 and Schwerdtner, 1964, p. 1217). The error introduced in this measurement by the difference in refractive index between the hemisphere (N = 1.649) and the crystal is negligible (Schwerdtner, 1964, p. 1217). Intersections of (010) and (110) were corrected such that the angle between c and z was 17°.

Structural Measurements - The orientation of the hornblende grains was measured from a thin section cut parallel to the prominent foliation. The c-axes of 150 grains were inclined at less than 25° to the foliation plane. The apparent elongation of measured grains was also determined and found, in all cases, to be closely parallel to the c-axis.
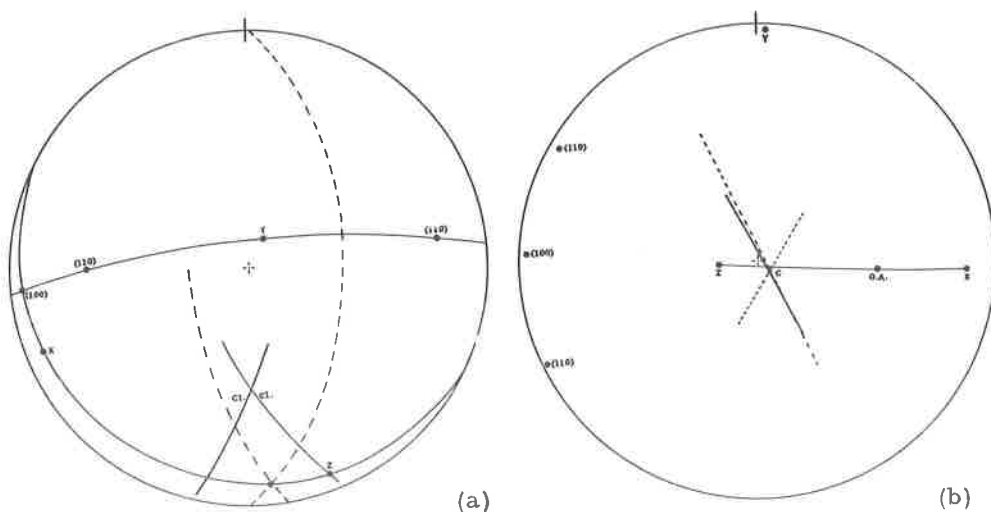
4

Figure 3. (a) Crystallographic parameters of a hornblende crystal section inclined at a large angle to (001), showing the large error in the determination of the c-axis when using the intersection of the cleavage (cl) or (010) and (110).

(b) Angle between c and Z (17°) obtained from a section parallel to (001). The position of the c-axis is determined from the cleavage intersection and intersection of (010) and (110).

Despite the pronounced anisotrophy of the hand specimen, a random distribution of X-, Y-, and Z-axes and the crystallographic c-axes was obtained on a summary diagram. Since the field study and the mesoscopic analysis (Abdel-Khalek and Khoury, 1971) indicate that the rocks have been affected by multiphase deformation, the microscopic data was subdivided into three separate groups. Group I, c-axes parallel to the subhorizontal lineation (L_2), plunging from 0° to 25°. Group II, c-axes parallel to the moderate to steep lineation (L_1), plunging between 25° and 70°. Group III, c-axes parallel to the subvertical lineation (L_3) plunging from 70° to 90°. The preferred orientation of the crystallographic and optic axes in each group became more evident (Figure 4a, b, and c). The X- and Y-axes are concentrated in bands that reflect the crystal symmetry of hornblende and indicate that {110} is predominantly subparallel to the ab fabric plane. A thin section cut perpendicular to the foliation and $\overline{b}_1 = L_1$, from another hornblende gneiss sample, shows that the c-axes of basal sections are subparallel to L_1 and that the X- and Y-axes form separate peripheral concentrations (Figure 4d).

5

Figure 4. (a) Stereographic plot of the optical and crystallographic parameters of 26 grains with c-axes parallel to the subhorizontal lineation (L_2).

(b) Stereographic plot of the optical and crystallographic parameters of 49 grains with c-axes parallel to the moderate to steep lineation (L_1) plunging to the northeast. Measurements of 19 grains plunging to the southwest, corresponding to L_1 (Abdel-Khalek and Khoury, 1971, fig. 7), were omitted.
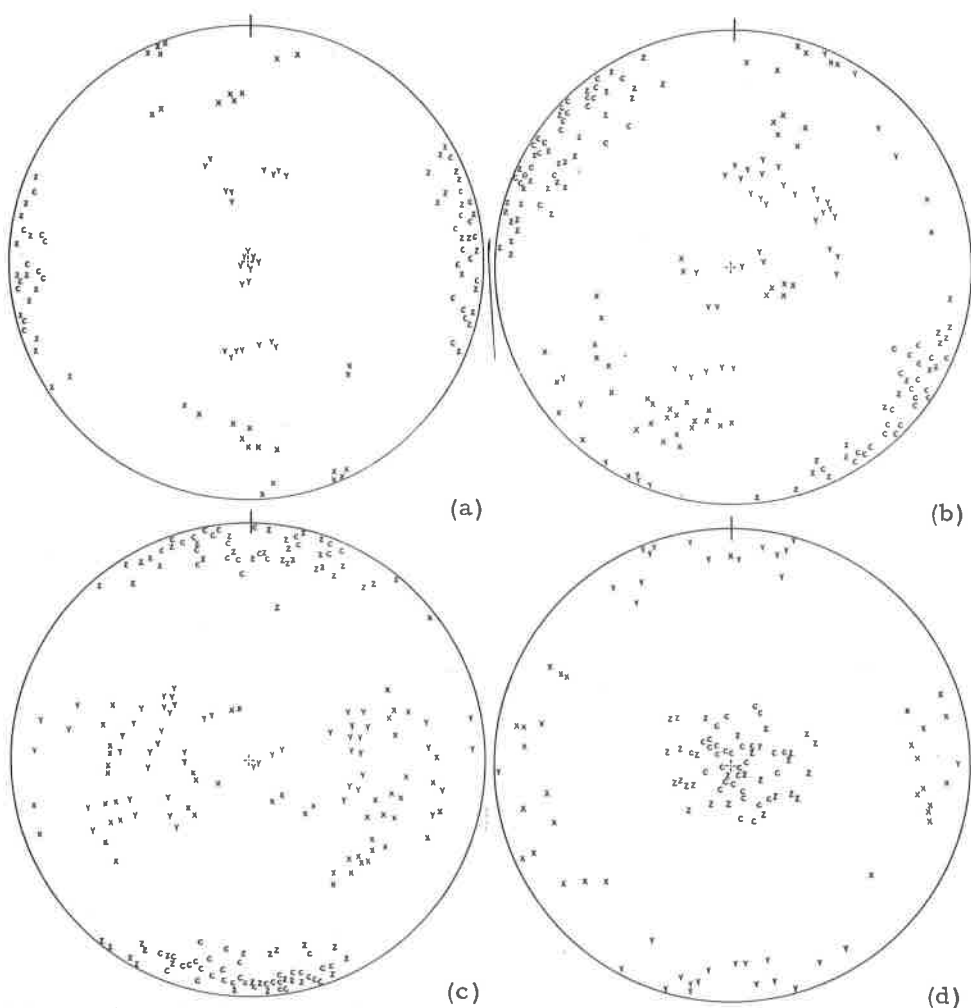
(c) Stereographic plot of the optical and crystallographic parameters of 56 grains with c-axes parallel to the subvertical lineation (L_3).

(d) Thirty measurements from a thin section cut perpendicular to the foliation and $b_1 = L_1$ showing that the X- and Y-axes form separate peripheral concentrations. The sample was collected near the intersection of Rts. 643 and 705.
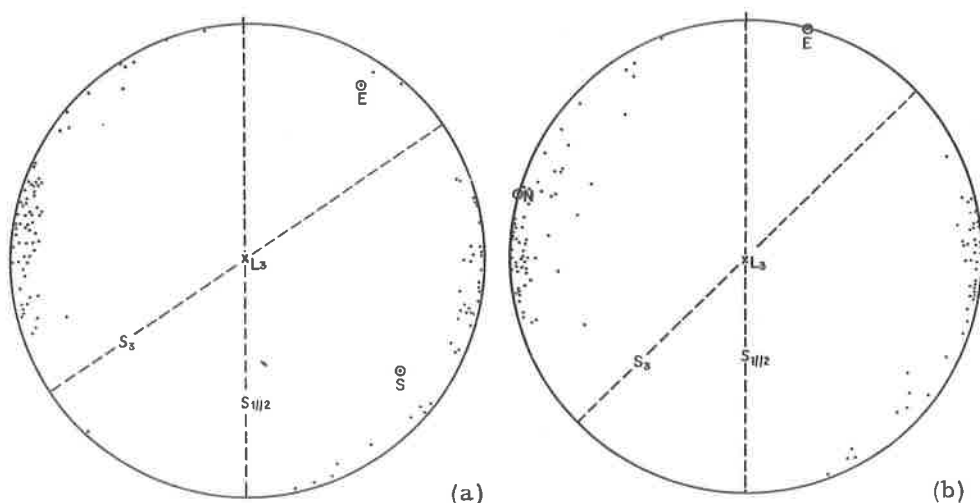
6

Figure 5. (a) Projection on the lower hemisphere of 91 poles to the (001) cleavage in mica. The thin section is cut at right angle to the lineation L_3 in phyllite. The sample was collected off Rt. 683, approximately 4 miles south of its intersection with Rt. 29 S.

(b) Projection on the lower hemisphere of 102 poles to the (001) cleavage in mica. The thin section is cut at right angle to the lineation L_3 in mica schist. The sample was collected south of New London, near the intersection of Rts. 623 and 625.

The Mica Subfabric

Samples of phyllite and a mica schist were studied. The samples are well foliated $S_1//S_2$,* have a cross-cutting slip cleavage (S_3) and a strong, steeply plunging crenulation lineation oriented approximately parallel to the direction of dip of the foliation. Small mica flakes can easily be detected parallel to this lineation which has been identified as L_3 (Abdel-Khalek and Khoury, 1971, fig. 7).

The attitudes of normals to the (001) cleavage of mica were determined according to the procedures described by Turner and Weiss (1963, p. 224-25). The maximum concentration of poles is normal to the regional foliation ($S_1// S_2$). A submaximum occurs normal to the axial plane slip cleavage (S_3). Moreover, the poles to (001) are dispersed in a girdle whose axis coincides with the well-developed lineation L_3 (Figure 5a and b). These relationships indicate that the orientation-patterns of mica reflect the presence and symmetry of the mesoscopic S-surfaces ($S_1// S_2$ and S_3) and lineation (L_3) in the two rock

---

*The foliation S_1 and cleavage S_2 are subparallel in this area (Abdel-Khalek and Khoury, 1971, p. 712).
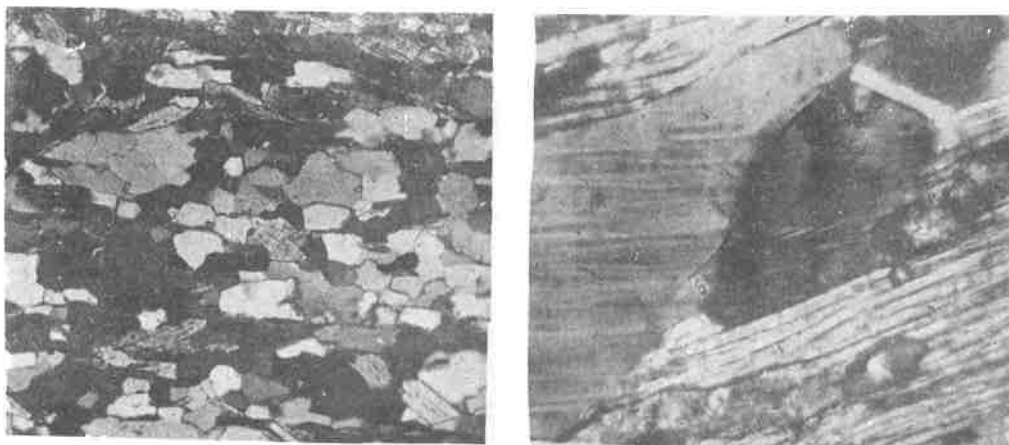
7

Figure 6. (a) (left) Phyllite showing clear, unstrained, granular quartz. The mica is predominantly parallel to $S_1//_2$ (E. -W.), with crystals oriented parallel to S_3 (NW. -SE.). Crossed nicols, longest dimension of photograph represents 1 mm.
(b) (right) Mica schist showing strained quartz with wavy extinction. Deformation lamellae extend across the grain boundary. Crossed nicols, longest dimension of photograph represents 1/4 mm.

groups. The crystallization of mica was predominantly parallel to the regional foliation and cleavage $S_1//S_2$, but some later reorientation took place parallel to the axial plane slip cleavage of the concentric flexural folds (Figure 6a and Abdel-Khalek and Khoury, 1971, Fig. 4c).

The Quartz Subfabric

The same phyllite and another mica schist specimen were used in determining the optic orientation of quartz in these two rock groups. The orientation of the optic axis (0001) was measured and plotted according to the method described by Turner and Weiss (1963, p. 202-3). Two oriented thin sections were cut perpendicular to the foliation of the phyllite. The first was cut normal to L_3, while the second was cut at a right angle to the strike of the sample. The rotation of the contoured diagram of the second thin section to the plane of the first produced a diagram identical to that measured and contoured directly from the first thin section. This indicates that the fabric of this rock sample is homogeneous with respect to quartz at the scale of a thin section (Knopf and Ingerson, 1938, p. 253). Both directly measured and rotated optic axes were combined in one diagram representing a cut normal to L_3. A maximum and several elongated submaxima suggest either a cleft girdle pattern of large apical angle and a girdle axis coinciding with L_3, or a crossed-girdle pattern with the poles of the girdles symmetrically

8

disposed about L_3 (Figure 7a). Therefore, the study of this diagram alone does not unambiguously clarify the relationship between microscopic and mesoscopic structural elements.

The section cut at right angles to the strike of the sample and subparallel to L_3 produces a crossed-girdle pattern of monoclinic symmetry. The plane of symmetry is at a right angle to $S_1//S_2$ (Figure 7b). An additional thin section, cut at a right angle to the foliation and at $45°$ to the strike and dip = L_3 of the sample, also results in a crossed-girdle pattern of monoclinic symmetry. The plane of symmetry is again at right angle to $S_1//S_2$ (Figure 7c). The crossed-girdles intersect at an acute angle of about $60°$ in both cases and the patterns show a strong tendency toward a symmetry of higher order - orthorhombic (Figure 7b and c).

Sylvester and Christie (1968, p. 577) have concluded that the intersection of the crossed-girdles is parallel to the intermediate principal axis of the strain ellipsoid and that the greatest and least principal axes of the strain ellipsoid bisect the angles between the girdles. If the direction of strike of the sample is taken to represent the approximate trend of the subhorizontal lineation L_2, as already established from field studies (Abdel-Khalek and Khoury, 1971, p. 712), then it can be seen that the intersection of the girdles is subparallel to L_2. Furthermore, this orientation is parallel to the axis of the asymmetrical flexural folds F_2 (Abdel-Khalek and Khoury, 1971, Figure 8c).

Turner and Weiss (1963, p. 432) suggested that syntectonic recrystallization of quartz produces patterns whose symmetry approximates that of the stress system. They equated the three mutually perpendicular directions of intersection of the planes of near symmetry, in and orthorhombic quartz sub-fabric, with the axes of principal stress σ_1, σ_2, and σ_3. The clear, unstrained granular quartz crystals (Figure 6a) showing a strong preferred optical orientation, controlled by the stress system prevailing during the period of asymmetrical flexural folding (F_2) suggest syntectonic recrystallization of quartz in the phyllite. The effects of either earlier and (or) later deformations cannot be readily detected in the petrofabric diagrams (Figure 7b and c). In addition, the maximum elongation of quartz grains was measured from three thin sections of different orientations. These measurements show that the strong optical alignment of quartz is not accompanied by any significant preferred elongation (Figure 8a, b, and c). Therefore, it can be tentatively concluded that the tendency toward orthorhombic symmetry of the quartz subfabric in the phyllite approximates the symmetry of the stress system during the development of F_2. The intersection of the crossed-girdles is parallel to σ_2, while σ_1 bisects the acute angle and σ_3 bisects the obtuse angle between the girdles (Figure 7b and c). An additional and independent restriction is that the maximum principal stress should also be perpendicular to $S_1//S_2$.

The orientation of the optic axis (0001) of quartz, in the mica schist, was studied from a section cut normal to the foliation $S_1//S_2$

9
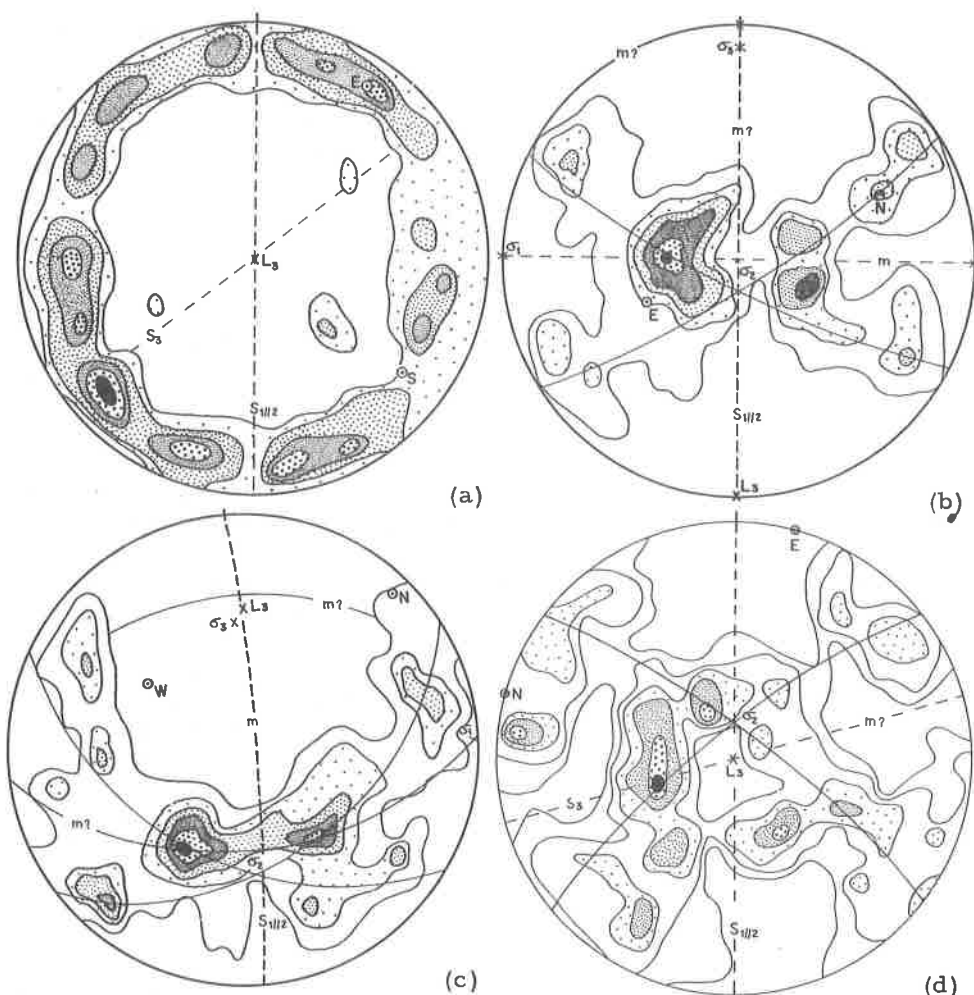
Figure 7. (a) Projection on the lower hemisphere of 700 quartz optic axes from a phyllite sample. Contours are at 1, 1 1/2, 2, 2 1/2, and 3 percent. S and E are geographic coordinates. (b) Projection on the lower hemisphere of 300 quartz optic axes from a phyllite sample. The thin section is cut at right angle to the strike and parallel to L_3. Contours are at 1, 2, 3, 4, 5, and 6 percent. N and E are geographic coordinates. σ_1, σ_2, and σ_3 are the principal stresses and m is a plane of symmetry. (c) Projection on the lower hemisphere of 200 quartz optic axes from a phyllite sample. The thin section is cut at right angle to the foliation and at 45° to the strike and dip. Contours are at 1, 2, 3, 4, 5, and 6 percent. N and W are geographic coordinates. σ_1, σ_2, and σ_3 are the principal stresses and m is a plane of symmetry.

10

and lineation (L3). The quartz grains show many strain effects express-
ed by fragmentation, wavy extinction and deformation lamellae (Figure
6b). The lamellae are subperpendicular to the undulatory extinction
zones and in some casss cross the boundaries of the grains, indicating
that they are of late tectonic development (Figure 6b).

If the distribution of maxima is considered in detail, the pattern
of preferred orientation of [0001] is triclinic. However, there is a
close approach to symmetry of a higher order -- monoclinic or even
orthorhombic. The crossed-girdles intersect at right angle and their
intersection is parallel to σ_2 and subparallel to the lineation L3 (Fig-
ure 7d).

The quartz deformation lamellae which occur in this sample are
similar to those which have been described in the literature from other
areas. The angle between the pole of the deformation lamellae and the c-
axis, in the grains containing lamellae, varies between 0° and 45°, with
a strong maximum between 5° and 15° (Figure 9). This histogram is
similar to the ones obtained by Fairbairn (1941), Christie and Raleigh
(1959), Hansen and Borg (1962), Nemec (1968) and Sylvester and Christie
(1968). The lamellae seem to develop only in the grains that plot at
the extremities of the crossed-girdles (compare Figure 7d and Figure
10a), implying that these grains are the ones that are suitably oriented
so that there is a high resolved shear stress parallel to [0001]. The
contoured diagram of the poles to the lamellae results in a double maxi-
ma pattern. The two maxima are approximately at right angles (Figure
10b). This pattern agrees well with that deduced by Carter and others
1964, p. 729) for rocks which have been subjected to a general state of
stress ($\sigma_1 > \sigma_2 > \sigma_3$).

Recent investigations of natural as well as artificially prepared
tectonites have shown that the planes containing poles of subbasal lamel-
lae and [0001] axes of the same grains pass approximately through a uni-
que axis which has been identified as the axis of greatest compressive
stress (σ_1). The poles of lamellae tend to lie nearer to it than the
[0001] axes (Christie and Raleigh, 1959; Hara, 1961; Carter and others,
1964 and Nemec, 1968). Therefore, if one considers the arrows on
Figure 10a as vectors, the position of σ_1 and σ_3 can be determined by
bisecting the angle between the appropriate maxima on Figure 10b. The
position of σ_2 is determined at right angle to the σ_1 - σ_3 plane (Fig-
ure 10b). An interesting result is that this position of σ_2 is subparallel

---

Figure 7. (d) Projection on the lower hemisphere of 240 quartz optic
axes from a mica-schist sample. The thin section is cut at
right angle to L3. Contours are at 1/2, 1, 1 1/2, 2, 3, and
4 percent. N and E are geographic coordinates. σ_2 is the
intermediate principal stress and m is a plane of symmetry.
The sample was collected off Rt. $\overline{24}$ approximately 1/2 mile
east of its intersection with Rt. 711.

Longest dimension of quartz grains

(a)

(b)

(c)
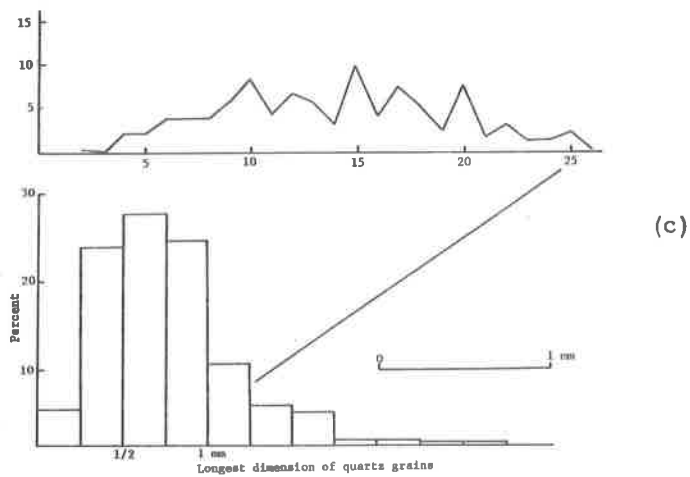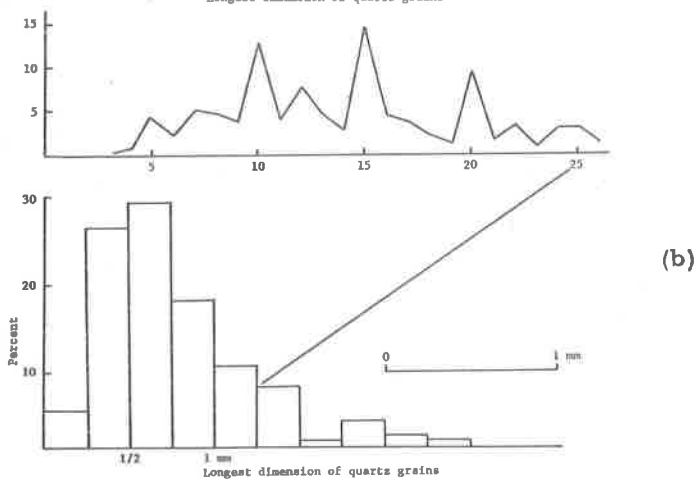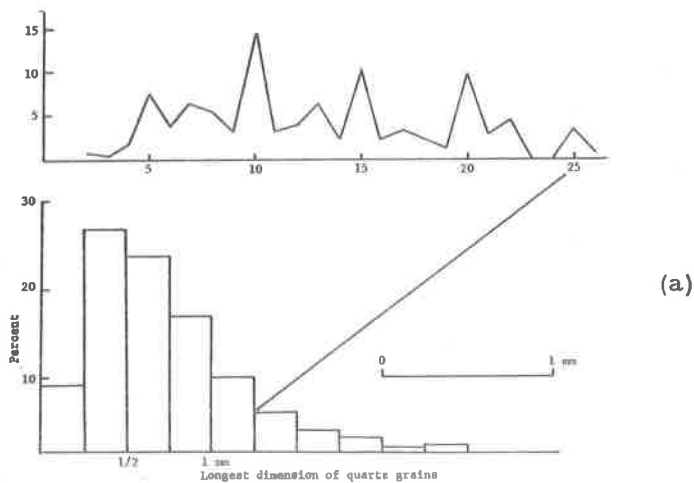
and agrees well with the one independently determined by the intersection of the crossed-girdles on the [0001] axis diagram (Figure 7d). The orientation of σ_1 also agrees well with it's direction as inferred from field studies (Abdel-Khalek and Khoury, 1971, p. 715). These relationships indicate that the deformation which produced the lamellae has also been responsible for the preferred orientation of the [0001] axes, and that the identified stress system is the one which was active during the period of open flexural folding (F_3).

DISCUSSION

The purpose of this preliminary investigation is to demonstrate that the microscopic fabric analysis has complemented the field studies and has provided additional detailed information that could not have been obtained from the study of the mesoscopic and macroscopic fabrics alone. In addition, each subfabric studied seems to record certain details of the deformation better than, or in preference to, others.

The hornblende subfabric and the mesoscopic structures were found to be generally homotactic, with groups of grains parallel to L_1, L_2 and L_3. The phyllites and mica-schists have similar mica subfabrics reflecting the orientation of the prominent foliation $S_1//S_2$ and to a lesser extent that of the cleavage S_3. The poles to (001) define a subhorizontal girdle whole axis coincides with L_3. Quartz seems to be a sensitive indicator of the intensity and orientation of the prevailing stress field. The preferred orientation of quartz is pronounced and its subfabric seems to be symmetrical to the principal strains and stresses in this area. The quartz subfabric of the phyllite appears to be controlled by the orientation of the stress system which was active during F_2 folding. The quartz subfabric of the mica schist is predominantly influenced by the stress system which was responsible for the development of the F_3 folds.

The alignment of small mica flakes parallel to L_3 (p. 1) and the mica subfabric, showing some reorientation of mica parallel to S_3 (Figure 5a and 6a), indicate that the phyllites have also been affected by F_3 folding. Therefore, it is reasonable to suggest that the intensity of the F_3 deformation must have been variable in this area.

Figure 8. The longest dimension of quartz grains in phyllite from three thin sections:
    (a) section cut at right angle to the foliation and the strike (403 measurements).
    (b) section cut at right angle to the foliation and the lineation L_3 (450 measurements).
    (c) section cut at right angle to the foliation and at 45° to the strike and lineation L_3 (435 measurements).
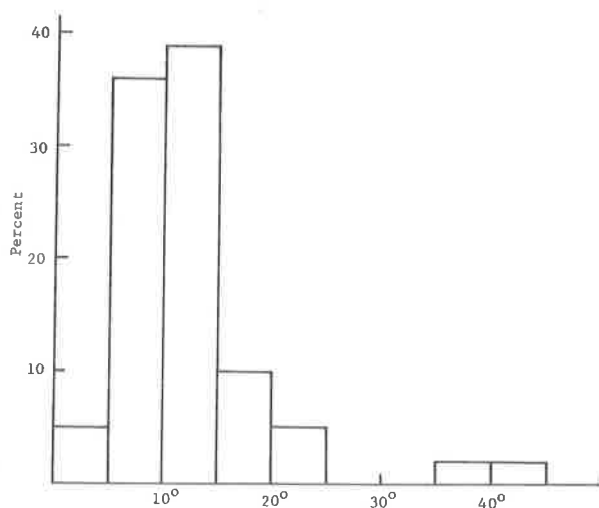
Figure 9. Histogram showing the variation in the angle between (0001) axes and the poles of deformation lamellae shown in Figure 10a.

(a)   (b)
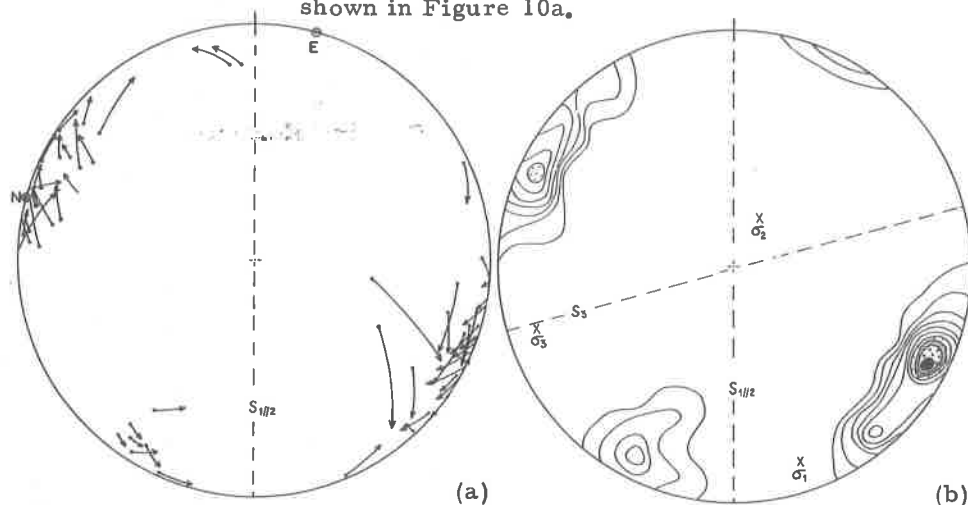
Figure 10. (a) Poles of deformation lamellae, heads of arrows, and (0001) axes of the same grains, tails of arrows, in quartz from Figure 7d.

(b) Poles of deformation lamellae in quartz from Figure 10a (50 measurements) contoured at 2 percent interval. The maximum is 18 percent. N and E are geographic coordinates. σ_1, σ_2, and σ_3 are the principal stresses.

14

The mesoscopic structural elements and the mica subfabric have been studied across the Catoctin Mountain-Blue Ridge anticlinorium in Central Virginia (Griffin, 1971). The mica fabric of the Chilhowee group there appears to reflect the effect of the F_2 folds. The mica fabric of Griffin's basement complex reflects the influence of both the F_2 and F_3 folds. This interpretation favors the additional fitting of a sub-horizontal girdle to the mesoscopic foliation and the statistical tendency toward the presence of that girdle has been recognized by Griffin (1971). The fabric of the Piedmont rocks shows the superposed effects of the two periods of deformation (F_2 and F_3) (Griffin, 1971, Fig. 5). This close correspondence between the mesoscopic fabric elements and the mica subfabric in the two areas implies a uniform structural evolution for the portion of the Inner-Piedmont and Blue-Ridge that extends from Bedford to the north of Lovingston, Virginia. It is also interesting to note in this respect that Cloos (1971) has also emphasized the consistency and uniformity of the deformation plan along the Western edge of the Blue-Ridge, from Pennsylvania to the James River, in Virginia.

REFERENCES

Abdel-Khalek, M. Lofti and Khoury, S. G., 1971, Structural and metamorphic evolution of the Otter River area, west-central Piedmont, Virginia: Geol. Soc. America Bull., v. 82, p. 707-716.

Briegleb, D., 1966, Beitrag zur Typisierung geregelter Hornblendetektonite: neues Jahrb. Min., Mh., p. 309-318.

Carter, N. L., Christie, M. J. and Griggs, D. T., 1964, Experimental deformation and recrystallization of quartz: Jour. Geology, v. 72, p. 687-733.

Christie, J. M. and Raleigh, C. B., 1959, The origin of deformation lamellae in quartz: Am. Jour. Sci., v. 257, p. 385-407.

Cloos, Ernst, 1971, Microtectonics along the Western Edge of the Blue Ridge, Maryland and Virginia: The Johns Hopkins Press, 234 p.

Fairbairn, H. W., 1941, Deformation lamellae in quartz from the Ajibik formation, Michigan: Geol. Soc. America Bull., V. 52, p. 1265-1278.

Griffin, V. S., Jr., 1971, Fabric relations across the Catochin Mountain-Blue Ridge anticlinorium in central Virginia: Geol. Soc. America Bull. v. 82, p. 417-432.

Hansen, E. C. and Borg, I. W., 1962, The dynamic significance of deformation lamellae in quartz of a calcite-cemented sandstone: Am. Jour. Sci., v. 260, p. 321-336.

Hara, I., 1961, Dynamic interpretation of the simple type of calcite and quartz fabrics in the naturally deformed calcite-quartz vein: Jour. Sci. Hiroshima Univ., ser. C, v. 4, p. 35-53.

Hess, H. H., 1949, Chemical composition and optical properties of common clinopyroxenes: Am. Mineral., 34, p. 621-666.

Knopf, E. B. and Ingerson, E., 1938, Structural petrology: Geol. Soc. America, Memoir 6, 270 p.

Nemec, D., 1968, On the mutual orientation of lamellae poles and 0001 axes of quartz in tectonites: Jour. Geology, v. 76, p. 358-364.

Schwerdtner, W. M., 1964, Preferred orientation of hornblende in a banded hornblende gneiss: Am. Jour. of Sci., 262, p. 1212-1229.

Sylvester, A. G. and Christie, J. M., 1968, The origin of crossed-girdle orientation of optic axes in deformed quartzites: Jour. Geology, v. 76, p. 571-580.

Troger, W. E., 1959, Optische Bestimmung der gesteinsbildenden Minerale, Teil I, Bestimmungstabellen, E. Schweigerbart'sche Verlagsbuchhandlung, Stuttgart, 147 p.

Turner, F. J., 1942, Determination of extinction angles in monoclinic pyroxenes and amphiboles: Am. Jour. Sci. 240, p. 571-583.

Turner, F. and L. Weiss, 1963, Structural analysis of metamorphic tectonites: New York, McGraw-Hill, 545 p.

Winchell, A. N. and H. Winchell, 1951, Elements of optical mineralogy, 4th ed., New York, Wiley, 551 p.

THE EFFECT OF HYDROLOGIC FACTORS ON THE PORE WATER CHEMISTRY OF INTERTIDAL MARSH SEDIMENTS

By

Leonard Robert Gardner
Department of Geology
University of South Carolina
Columbia, South Carolina 29208

ABSTRACT

Investigation of the pore water chemistry of marsh sediment near Georgetown, South Carolina reveals that three hydrogeochemical settings play a role in determining the chemical parameters of interstitial waters in the intertidal marsh environment. In areas of the marsh remote from both tidal creeks and sources of fresh ground water (e.g. partially buried Pleistocene beach ridges) pore waters are hydraulically stagnant and characterized by high alkalinity (4-12 millimoles/liter) low pS (9.5-10.5) and moderate pH (6.6-6.7). The chemistry of such areas correlates approximately with a theoretical model for sulfate reduction in closed, inert sediment (Gardner, 1971, 1973). Adjacent to sources of fresh ground water the salinity and pH decrease but the $SO_4^=/Cl^-$ ratio rises. These marginal areas are usually comprised of sandy sediment which is probably well ventilated. The chemistry of these areas thus appears to be controlled by the oxidation of sulfide to sulfate. Interstitial waters along the banks and margins of tidal creeks are marked by high pH (6.8-7.5), low alkalinity (2-4 millimoles/liter) and normal salinity and $SO_4^=/Cl^-$ ratios. Such areas are hydraulically active settings where fresh seawater infiltrates at high tide, mixes with more reduced waters and subsequently drains at low tide. These findings should be borne in mind in any sampling procedure designed for the study of sulfate reduction or diagenesis in marsh sediments. The hydrologic control of pore water chemistry may also affect the distribution and/or vitality of marsh organisms.

INTRODUCTION

Although there is a considerable body of literature pertaining to sulfate reduction and the chemistry of interstitial waters from marine sediments, most of this work has been devoted to subtidal sediments where transfer of dissolved substances is affected by diffusion or compaction (Berner, 1971; Berner, 1966; Berner et al., 1970; Presley

17

and Kaplan, 1968). In the intertidal marsh, additional mechanisms of transfer are possible because of hydraulic gradients induced by the rise and fall of the tide and because of evapo-transpiration. The purpose of this paper is to show that such mechanisms can produce distinct variations in pore water chemistry and that analysis of these variations may in turn reveal unanticipated aspects of marsh hydrology.

METHODS OF STUDY

Field work for this study was conducted at the Baruch marsh near Georgetown, S. C. (Figure 1) during the summer of 1971. The marsh is an intertidal salt marsh typical of the South Carolina coast and is dominated by Spartina. The tidal range in this area is about 6 feet so that during low tide the water level in the tidal creeks is about 3 to 5 feet below the general level of the marsh mud.

Interstitial water samples were extracted from the marsh sediment at various locations by means of an aluminum tube with a perforated fitting at one end. Upon insertion into the marsh sediment pore water samples were drawn into the tube by means of the suction produced by withdrawal of a tight fitting piston from the tube. The samples were then stored in BOD bottles to prevent escape of dissolved gases during transport to the laboratory. In the laboratory measurements of pH, Eh, $pS^=$, and alkalinity were obtained, usually within six hours after collection. Later, measurements of salinity and $SO_4^=$ were obtained from filtered aliquots of the original samples. Electrode methods were employed for measurement of pH, Eh, and $pS^=$. Alkalinity was determined by titration with 0.1N H_2SO_4 and $SO_4^=$ was determined gravimetrically by precipitation with $BaCl_2$. Salinities were determined with an American Optical Corporation temperature compensated optical refractometer. Chloride concentrations were calculated from salinity values on the assumption that salinity is due mainly to Na^+ and Cl^-.

To study the effect of salinity variations and boundary effects on the chemistry of interstitial waters a series of samples was taken along several lines of profile that trend roughly perpendicular to Goat Island and Clambank Creek (Figure 2). Goat Island is a partially buried Pleistocene beach ridge and contains potable fresh groundwater. Along the boundary between Goat Island and the marsh proper the marsh sediment
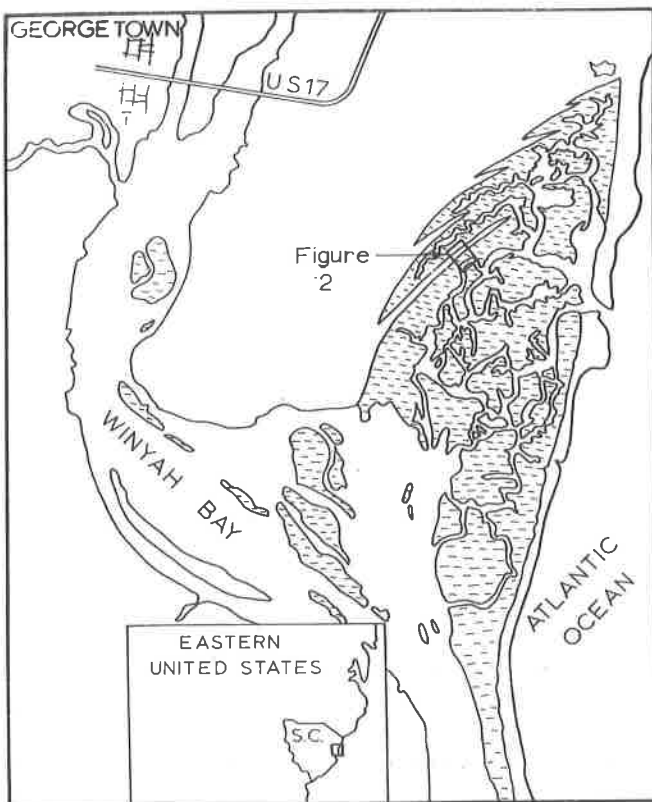
Figure 1. Location of Baruch Marsh and study
area.

consists of well sorted, medium sand. This margin of sandy marsh
sediment extends 50 to 100 feet out from the eastern edge of Goat Is-
land into the marsh proper. Beyond the margin of sandy sediment, the
marsh sediment consists of dark gray, organic, rich mud. Along the
Clambank Creek (and other creeks) the marsh proper terminates abrupt-
ly at the rather steep banks of the creek which are exposed at low tide.
Groundwater level measurements at low tide indicate that the water
table of the marsh is essentially horizontal throughout most of the
marsh but that at about 10 feet from the creek banks it begins to slope
steeply towards the creeks. Thus the margin of the marsh adjacent to
the tidal creeks is hydraulically dynamic compared to interior regions.
The profiles therefore pass through three regions: (1) the marginal
sandy region adjacent to sources of fresh groundwater, (2) the stagnant
interior region, and (3) the hydraulically dynamic region adjacent to the
tidal creeks. As will be seen the pore water chemistry of each region
is distinct from that of other regions.
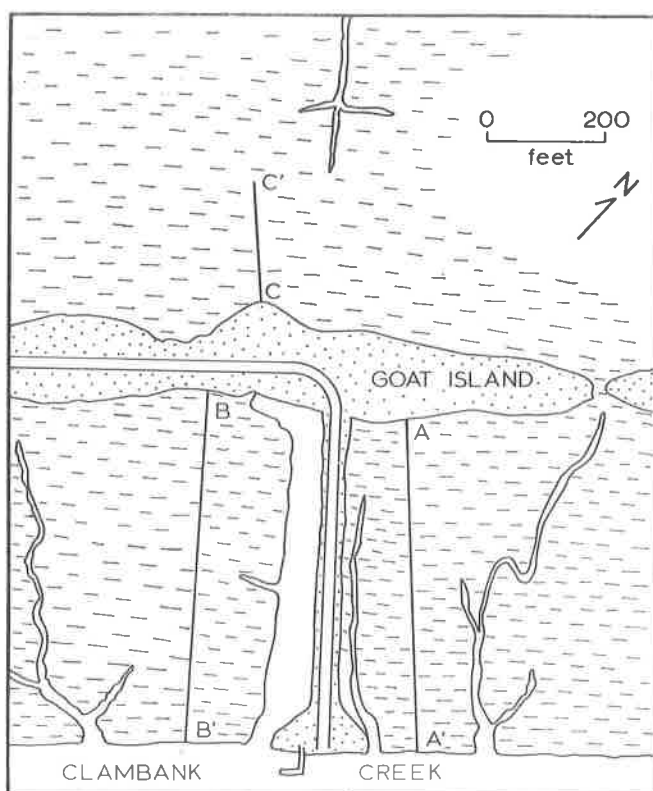
Figure 2. Location of profiles shown in Figure 3.

RESULTS AND DISCUSSION

The results of the profile studies are shown in Figure 3 and Table 1. Inspection of the figures reveal the following general features of pore water chemistry among the three hydrologic environments between Goat Island and the tidal creeks.

	Margins of Tidal Creeks	Interior of Marsh	Sandy Margin Along Goat Island	Surface Seawater
pH	6.55 to 7.30	6.60 to 6.75	5.90 to 6.60	8.0-8.1
Eh	-96 to +168	-80 to -174	-94 to +112	+290 to +340
pS	10 to 12	9.8 to 11.0	11.25 to 14.25	-
Alkalinity (ppm $CaCO_3$)	270 to 360	300 to 1200	140 to 380	115
Salinity (ppt)	31 to 36.5	34.5 to 48.5	29 to 53	30 to 36
SO_4^-/Cl	.143	.130 to .150	.148 to .173	.143

A 1   10   100   200   MHT   300   400   500   **A'**

DEPTH (ft)

```
                                              6.67
5.89    6.00   6.26               6.72       10.22              6.79  6.72
13.79  12.27  11.25  6.62        10.05       -128      6.79 10.19 11.20
  +19   -57    -94  10.10                    460      10.19 -151  -75
  140   170   290   -139  6.72   6.72        34.5      -151 600  360
  290  33.0  41.5  680  10.05  10.07         .142      600  35.0 335
  155  .161  158   36.5  -157   -113               MUD 35.0 -138- 153
  6.29        140   .141  500   35.5            SAND  6.57
 22.77  .156        355   35.5           6.62        10.36
  +112                                  10.20        -126
  140                                   -120         385
  280                                   440          35.0
                                        34.5         .143
                                        .141
```

B   MHT   **B'**

DEPTH (ft)

```
        6.21                                  6.70
6.29  12.42  6.19   6.21  6.67        6.65    10.75        6.74  6.60
12.52  -58  12.14  12.02 10.28       10.18    -103        11.05 11.30
 200   -56  6.63   -63   -151  6.63   -132   -305-  6.63  -103  -77-
 240  360  230   300   845  10.20    535     330  10.28 -300 315
 360  160  365   39.5  380  -156    35.0    148  -126 33.5 33.0
36.0      .156   159   725   6.59   158     430  11.56 .152 158  6.56
.153              .355 10.40         35.0   -80  320      12.00
                       -140          .138   345            -58
                       460                  6.51          2.40
                       34.5                               31.0
                       .148                               .154
```

C   MHT   **C'**

DEPTH (ft)

```
                          6.64
                         10.30   SAND
                         -157
5.96  5.90  6.18  6.40  1080.
14.25 12.90 1200 11.45   48.5   6.95   6.61
 +19  -63  -86   -87    .144   10.15  10.20
 175  145  325   380           -174   -159
 317  335  455   530    6.61   1040   1020
 173  172  .148  159   10.10   43.5   40.5
                        -165          .129
                        1085   7.35
                        44.5   9.87
                        .128  -181
                              1215   6.67
                              48.5  10.20
                                    -149
                                    965
                                    45.5
                                    .135
```
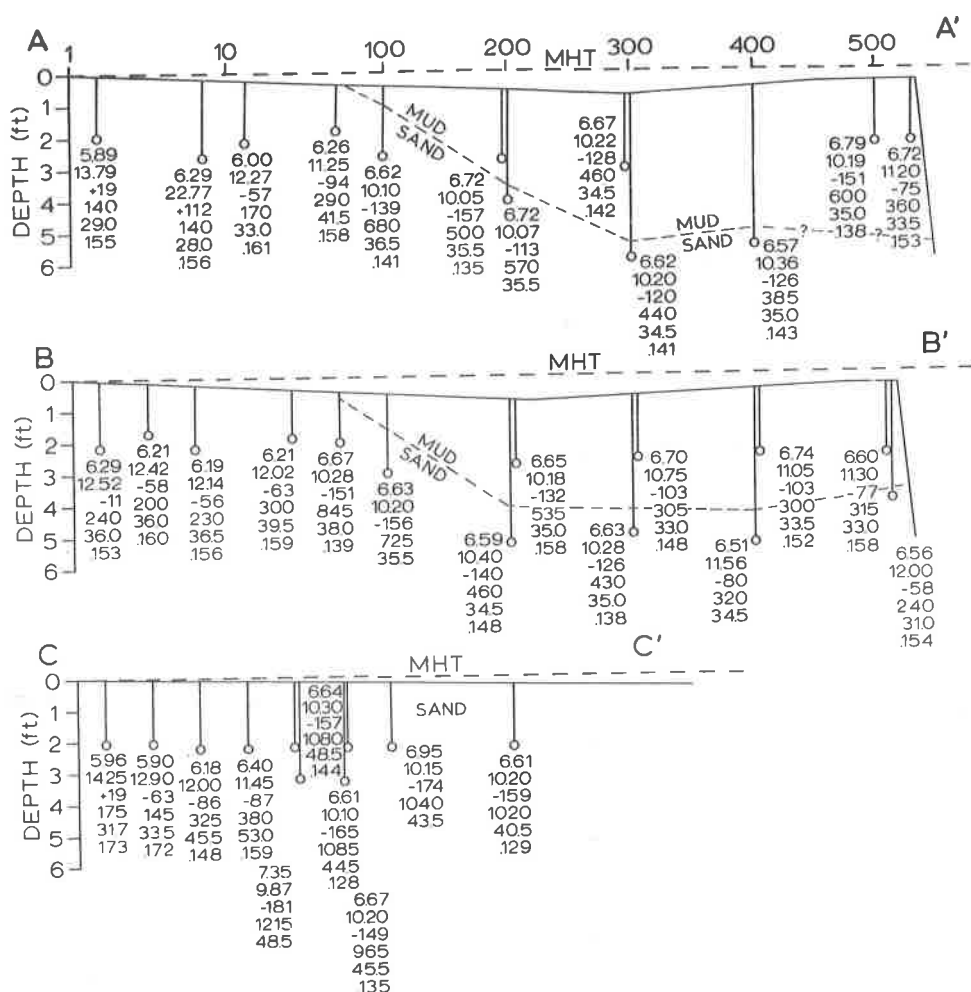
Figure 3. Profiles of interstitial water chemistry from Goat Island to tidal creeks. Numbers in columns at each sample site refer to pH, pS, E_h (in mv), alkalinity (as ppm $CaCO_3$), salinity (in ppt), and $SO_4^=/Cl^-$ ratio. Note that first hundred feet of profiles are shown on log scale in order to separate closely spaced samples near Goat Island.

The diagrams in Figure 4 show in a generalized fashion the variation of pertinent chemical parameters along a typical profile from Clambank Creek through Goat Island and form the basis for the following discussion.

Table 1. Vertical Profile of Interstitial Water Chemistry at 3 and 15 Feet from Creek Bank.

Location	Depth	pH	Eh	pS	Alkalinity (ppm CaCO$_3$)
3 feet	1.0 ft.	7.37	+168mv	17.0	270
"	1.5 ft.	7.00	-91	11.2	-
"	2.0 ft.	6.92	-78	11.0	295
"	2.5 ft.	6.95	-74	11.0	-
"	3.0 ft.	7.07	-96	10.4	-
"	3.5 ft.	7.10	-26	12.1	-
15 feet	1.5 ft.	6.68	-131	9.9	540
"	2.0 ft.	6.79	-135	10.0	-
"	2.5 ft.	6.71	-136	9.9	-
"	3.0 ft.	6.69	-132	10.0	515
"	3.5 ft.	6.89	-132	9.9	-

Interior of the Marsh

For profiles A-A' and B-B' (Figure 3) the interior of the marsh may be defined as the region extending from the first appearance of surface mud at the edge of the sandy margin to about 10 feet from the edge of the tidal creek. Within this region pH values lie generally between 6.6 and 6.7 and closely approach the asymptotic lower limit of pH reduction (6.62) for sulfate reduction in closed marine waters (Gardner, 1971). The relationship between pH and alkalinity (Figure 5) shows a distinct peak in alkalinity values at about pH 6.65, according with the predicted asumptotic lower limit of pH reduction. Also the theoretical curve for pH versus alkalinity in a closed marine system with inert sediment pass through the peak and high pH limb of the distribution. The samples in Figure 5 with lower pH values (below 6.6) come from the sandy margins of the marsh and in a few cases from buried sandy horizons near the margin of the tidal creek where hydrologic conditions produce departures from ideal closed system chemistry. Thus the interior of the marsh appears to be a region where sulfate reduction proceeds approximately as a closed system containing inert sediment. Two factors appear responsible for this behavior. The presence of mud at the surface of the marsh prevents rapid diffusion or flow of substances into or out of the system. Also the virtual absence of hydraulic gradients in this region prevents the rapid drainage of reduced waters out of the system and the influx of fresh seawater into the system. Thus the region is relatively stagnant and isolated.

Sandy Margin

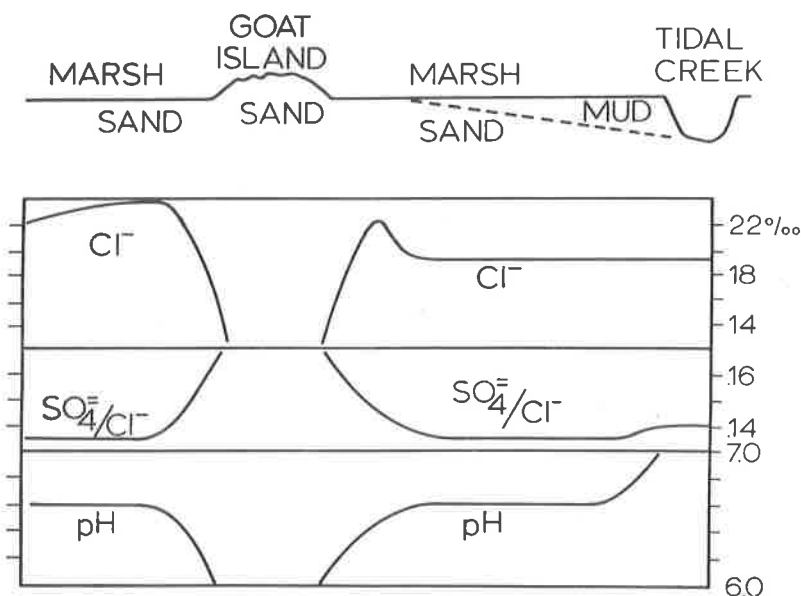The chemical changes that occur across the sandy margin from

Figure 4. Idealized profile of interstitial water chemistry from Goat Island to tidal creeks based on data of Figure 3 and Table 1.

the marsh interior to Goat Island may be summarized as follows:

1. Alkalinity and pH show marked progressive decreases.
2. The ratio of $SO_4^=$ to Cl^- rises markedly as does pS and E_h.
3. The salinity at first rises but then drops off near the margin of Goat Island.

These changes are the result of the interplay of several factors. The drop in salinity near the edge of Goat Island is obviously due to dilution with fresh groundwater. The rise in salinity near the outer edge of the sandy margin is probably due to the combined effects of evaporation and transpiration. At low tide, salinities as high as 46 °/o have been observed in small pockets and puddles on the marsh surface. In the sandy marsh, such waters have a much greater opportunity to infiltrate or diffuse into the marsh because the sediment is more permeable and because this portion of the marsh is exposed for longer periods between successive high tides. In this respect it is interesting to note that salinities in the sandy marsh on the west side of Goat Island (profiles C-C', Figure 3) are much higher than those on the east side possibly because the elevation of the marsh here is slightly higher and therefore its exposure between high tides is greater.

Several hypotheses can be proposed to explain the drop in pH from the marsh interior to Goat Island:

1. Dilution of reduced interior marsh water with fresh ground water from Goat Island.
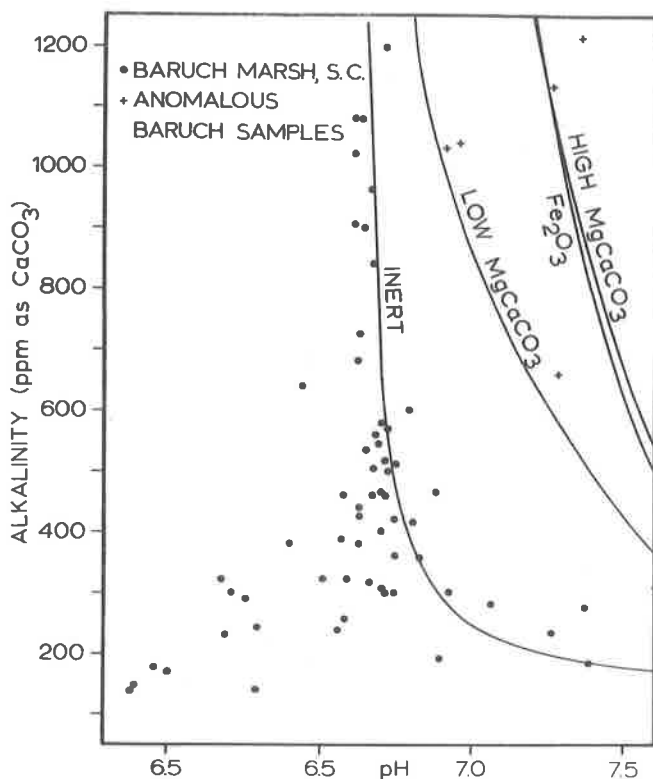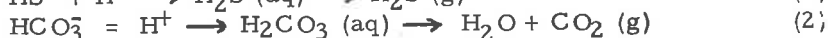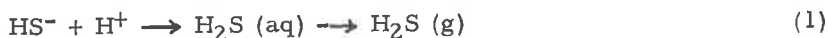
23

Figure 5. Alkalinity versus pH for interstitial water samples from Baruch Marsh. Solid lines represent theoretical variation of alkalinity versus pH for closed system sulfate reduction in (1) inert sediment, (2) $CaCO_3$ sediment, and (3) Fe_2O_3 sediment. Crosses indicate anamolous samples that are probably under influence of $CaCO_3$ or Fe_2O_3.

2. Diffusion of H_2S and CO_2 out of the reduced water in the sandy marsh.
3. Oxidation of sulfide due to the diffusion of O_2 into the permeable sandy marsh.

The data available at present indicates that the last hypothesis is probably the controlling mechanism for pH reduction in the sandy marsh. Dilution is an inadequate mechanism because the pH begins to drop at the outer edge of the sandy margin where salinity begins its initial rise. Also, experiments show that when normal reduced water from the marsh interior is mixed in varying proportions with fresh water the pH invariably rises. Experiments also indicate that when samples of normal reduced water are allowed to equilibrate with the atmosphere the pH again

24

rises, usually to values close to that of normal surface seawater. Thus diffusion of H_2S and CO_2 proceeds according to the following reactions:

$$HS^- + H^+ \longrightarrow H_2S \text{ (aq)} \longrightarrow H_2S \text{ (g)} \tag{1}$$
$$HCO_3^- = H^+ \longrightarrow H_2CO_3 \text{ (aq)} \longrightarrow H_2O + CO_2 \text{ (g)} \tag{2}$$

which indicates that the pH should rise with the escape of these gases.

The last hypothesis, oxidation of sulfide, is supported by the fact that the drop in pH in the sandy margin coincides with a rise in the $SO_4^=/Cl^-$ ratio from values near or slightly below the $SO_4^=/Cl^=$ ratio of surface seawater (0.141) observed in the marsh interior to values as high as 0.172 near the edge of Goat Island. At the present time it is not clear whether this rise in the $SO_4^=/Cl$ ratio is due to the oxidation of dissolved sulfide or solid phases such as FeS or FeS_2. Also it is not clear whether oxidation is due primarily to the vertical diffusion of atmospheric O_2 through the marsh surface or to the lateral diffusion of dissolved O_2 from the ground water beneath Goat Island out into the saline waters of the marsh. Several considerations, however, suggest that lateral diffusion is the dominant mechanism. Profile C-C' (Figure 3) shows that the low pH zone, due to oxidation of sulfide, extends about 15 feet into the sandy marsh and that beyond this point high salinities prevail despite the fact that the other chemical parameters are indicative of closed system sulfate reduction, similar to the interior regions of profiles A-A' and B-B'. This indicates that although the mud content of the sand may increase somewhat into the marsh the sand is still permeable enough for evaporative processes to produce high salinity water. Thus one would not expect the rate of vertical diffusion to be greatly reduced in this region. Therefore the oxidation of sulfides in this region is retarded not by the low permeability of the sediment but possibly because diffusing O_2 in the near surface zone is totally consumed by intense bacterial decomposition of organic matter which thus provides a barrier against O_2 penetration. Alternatively one could argue that the apparent lack of sulfide oxidation in this region is due simply to the fact that the rate of sulfate reduction here greatly exceeds the rate of vertical diffusion of oxygen.

Margins of Tidal Creeks

Observations of water levels in tubes inserted into the marsh near the margins of tidal creeks show that the ground water table of the marsh fluctuates with the tidal cycle, rising with high tide and falling with low tide. This zone of fluctuating groundwater levels generally lies within 15 feet of the margins of the tidal creeks. In the marsh interior groundwater levels never fall more than one inch below the surface of the marsh but along the margins the groundwater level may fall one or two feet below the marsh surface. Generally during low tide the average slope of the groundwater table along the margins of
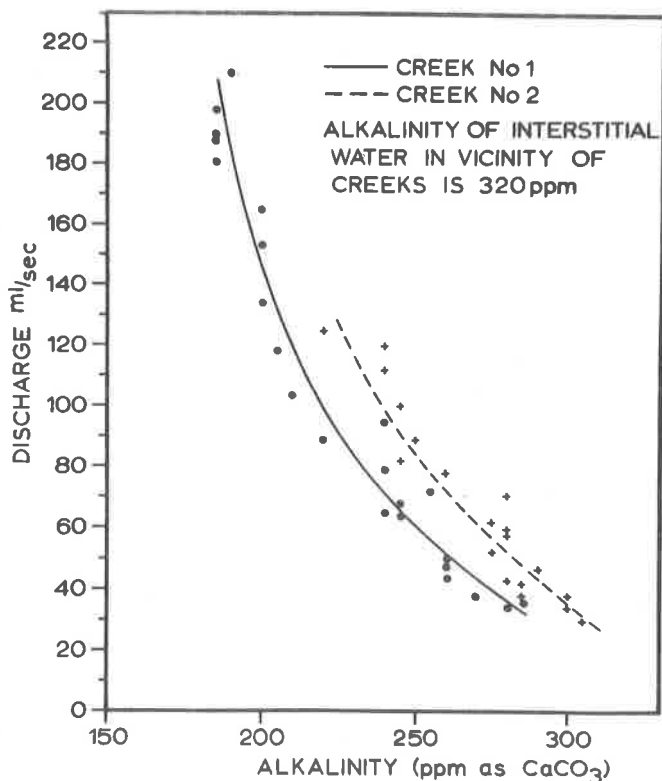
Figure 6. Alkalinity versus discharge for two
tidal trickles.

the tidal creeks is about 20 percent. Thus along the margins of the
tidal creeks there is active drainage of interstitial water from the marsh
during low tide and rapid infiltration of fresh seawater into the marsh
sediment during high tide. That active drainage of interstitial water
does occur during low tide is further indicated by the chemistry of low
tide trickles which show a progressive increase in alkalinity as low
tide is approached (Figure 6). This indicates that as low tide is ap-
proached the proportion of reduced interstitial water in the total flow
of tidal trickles progressively increases. Thus the interstitial com-
ponent of total flow is probably derived largely from the zone of fluctuat-
ing groundwater levels along the margins of tidal creeks.

Two mechanisms appear to control the chemistry of interstitial
waters in the zone of fluctuating groundwater levels: (1) mixing of high-
ly reduced interstitial waters from the marsh interior with fresh sea-
water which tends to produce waters with high pH (6.8-7.3) and low al-
kalinity (250-350 ppm $CaCO_3$) and (2) oxidation of sulfide which produc-
es waters with low pH (6.5-6.6) and low alkalinity (250-350 ppm $CaCO_3$).
The first mechanism is dominant in regions where the banks of the tidal

26

creek are composed entirely of mud, especially in the upper level of the marsh where mixing should be most intense. The data for the creek bank profile in Table 1 show this type of behavior. Where a buried sandy horizon intersects the creek bank (Profile B-B' and possibly A-A' of Figure 3) the interstitial water chemistry resembles that near the edge of Goat Island although the evidence for oxidation of sulfide is not as strongly developed. Apparently under these circumstances it is possible for dissolved oxygen in surface seawater to diffuse into the sandy horizon and cause oxidation of sulfide. Also where the sandy horizon lies below the range of fluctuating ground water levels the tendency for mixing should be greatly reduced thereby allowing the effects of oxidation to be manifest.

SUMMARY AND CONCLUSIONS

The results of this study demonstrate that hydrologic factors affect the chemistry of interstitial marsh water. The mechanisms that can cause deviations from the normal chemistry predicted for closed system sulfate reduction include (1) dilution with fresh water or fresh seawater, (2) evapo-transpiration, and (3) oxidation of sulfide. Normal closed system chemistry prevails in the interior regions of the marsh which are remote from sources of fresh groundwater as well as from the hydraulically active margins of tidal creeks. In such regions the absence of hydraulic gradients and the presence of relatively impermeable surface muds combine to produce a system relatively isolated from the atmosphere and hydraulically stagnant. Near the edges of partially buried Pleistocene beach ridges, dilution of marsh water with fresh ground water produces a reduction in salinity. Also diffusion of dissolved oxygen from the fresh groundwater into the marsh water causes oxidation of sulfide and a reduction of pH below the asymptotic lower limit of pH reduction predicted for normal closed system sulfate reduction. Between the edge of the Pleistocene beach ridges and the normal stagnant marsh interior there is generally a zone of sandy permeable sediment where evapo-transpiration causes the salinity to greatly exceed that of normal seawater. Along the margin of tidal creeks where groundwater levels fluctuate in response to tidal variation there is active mixing of reduced interstitial waters with fresh seawater. This causes a rise in pH and decrease in alkalinity. However where buried sandy horizons intersect the creek bank, diffusion of oxygen from surface seawater can cause oxidation of sulfide to produce interstitial waters similar to those found along the edges of Pleistocene beach ridges.

These results should be borne in mind in any sampling procedure designed to study sulfate reduction and diagenesis in marsh sediments. Also the hydrologic control of pore water chemistry may affect the distribution and vitality of marsh organisms. In this connection the author has observed that the growth of Spartina seems to be more luxuriant along the margins of tidal creeks than in the marsh interior.

27

REFERENCES

Berner, R. A., 1971, Principles of Chemical Sedimentology: McGraw-Hill, New York, 240 p.

_____, 1966, Chemical diagenesis of some modern carbonate sediments: Amer. J. Sci., v. 264, p. 1-36.

Berner, R. A., Scott, M. and Thomlinson, C., 1970, Carbonate alkalinity of the pore waters of anoxic marine sediments: Lerminol. and Oceanogr., v. 15, p. 544-549.

Gardner, L. R., 1971, Chemical models for sulfate reduction in closed, anerobic, marine environments: Abstracts with Programs, Geol. Soc. of America, v. 3, no. 7, p. 577.

_____, 1973, Chemical models for sulfate reduction in closed anaerobic marine environments: Geochim. et Cosmochim. Acta, v. 37, p. 53-68.

Presley, B. J. and L. R. Kaplan, 1968, Changes in dissolved sulfate, calcium and carbonate from interstitial water of near-shore sediments: Geochim. et Cosmochim. Acta, v. 34, p. 1037-1048.

DISTRIBUTION OF THE COREY SHAPE FACTOR IN

THE NEARSHORE ZONE

By

David Poche'
Anne Jones
Bruce Taylor

Department of Environmental Sciences
University of Virginia
Charlottesville, Virginia 22903

ABSTRACT

The Corey shape factor (SF) for several thousand sand grains were found to have a mean value of 0. 66. This is lower than the previously assumed value of 0. 70 which is commonly used for rapid sediment or granular metric analysis. This difference has the potential of an approximate 5 percent error in the estimation of the nominal size of any sand sample. Comparison with the shape factors of river sands (Schulz et al. 1954) indicate no significant differences between surf abrasion and fluvial abrasion for particles of sand size. Histograms of the data are presented for possible computer simulation purposes. The distribution of Zingg forms are also presented.

INTRODUCTION

Corey (1949) and McNown and Malaika (1950) devised a method for the characterization of particle shapes. This index of grain shape is the Shape Factor (SF).

$$SF = c/\sqrt{ab}$$

where a, b, and c are the mutually perpendicular axes of the grain; the largest axis is a and the smallest is c. A grain with a shape factor of 1. 0 would be a sphere; grains with shape factor less than 1. 0 would be non-spherical.

Rapid sediment or granularmetric analysis (Schlee, 1966; Brezina, 1969) usually assumes that naturally worn sediment has a mean shape factor of 0. 70 (Inter-agency Committee on Water Resources, 1958). The basis for this assumption was apparently an article by Schulz et al. (1954) in which several hundred fluvial particles ranging from large pebbles to sand were measured in order to determine the effect of their shape upon their hydraulic fall velocity. If the assumption

29

of mean shape factor is invalid then errors in the estimate of the nominal size of the sediment will result. Part of this study is aimed at checking this assumption.

This study was also conducted in order to determine if a significant difference exists between the mean shape factor of the sand grains found in the nearshore zone and similar grains found in rivers. If such a difference exists then there may be a difference in the abrasional history between these two environments. Dobkins and Folk (1970) showed that there is a difference between marine and fluvial pebble shapes. In general, they found that the roundness increases from rivers to beaches and the sphericity decreases. They observed that river pebbles of all sizes were substantially alike in all shape properties but that beach pebbles showed marked shifts in shape with changing pebble size. They attributed the shape differences between the two environments to differences caused by surf abrasion.

If abrasion is a significant process for sands of the nearshore zone then differences should exist in the population parameters of the distribution of Corey shape factor for sand grains of marine and fluvial environments. Grain shape may then be used as a paleo-environmental indicator.

MEASUREMENTS AND DATA

In order to take a representative sample of sand from the nearshore zone, four sets of samples were taken under four different wave conditions from a 700 foot pier located at Crystal Beach on the Gulf of Mexico near Destin, Florida (Figure 1). This coastline is classified as one of low to medium energy (Tanner, 1960). Studies of the beach and nearshore along this portion of the coast have documented that the sediments of this region exhibit uniform size ranges (Gorsline, 1963, 1966). The sediments of this locality are predominatly quartz with only 1 to 2 percent accessory minerals and shell fragments. They are ideal for the purposes of this study because of their uniformity of size and mineralogy. In each sample set, 20 samples were taken from the pier on thirty foot centers beginning with the swash zone and continuing to the end of the pier.

Each sample was split down to about 2 grams from which 200 grains were selected for measurement. The axial lengths of the grains were measured with the aid of a Lietz microprojector and a low power microscope mounted in the plane of the stage of the microprojector. The projected axes were measured to the nearest 0.05 mm, and the axis measured with the microscope was measured to the nearest 0.02 mm. Characterization of the populations of shape based upon the classification by Zingg (1935) were also made (Figure 2).

The distribution of Corey shape factors found from the four sample sets (80 samples)is shown in Figure 3.
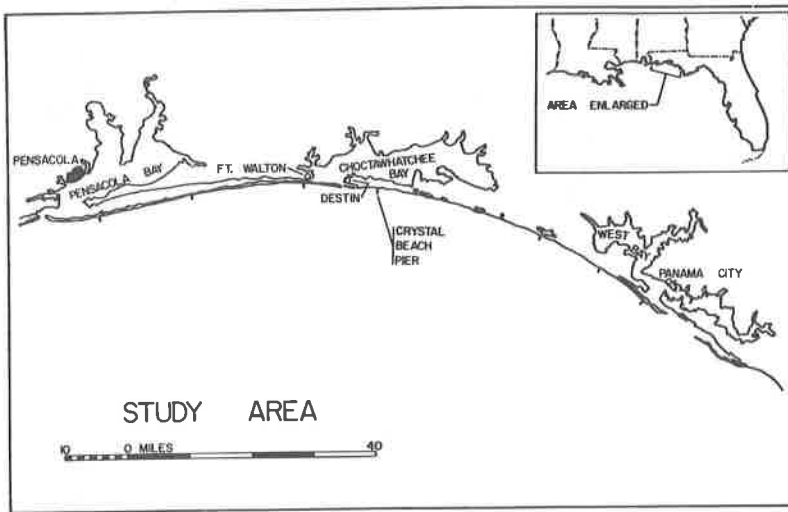
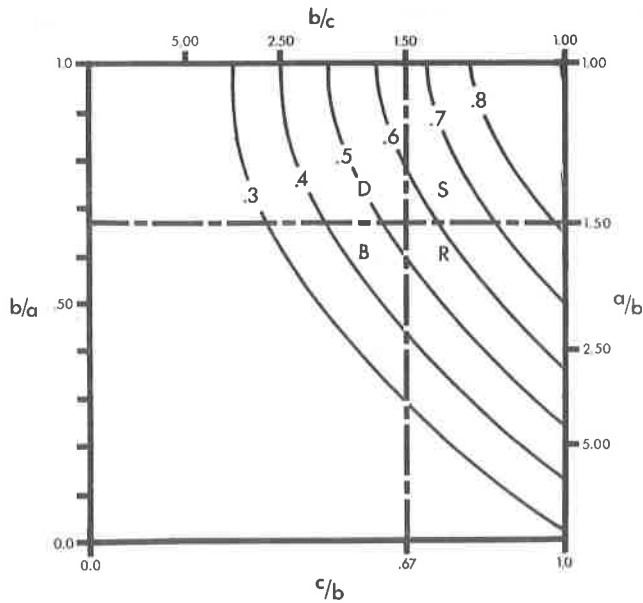Figure 1. Location of Crystal Beach pier.

Figure 2. Shape classification diagram. Various axial ratios are shown at side of diagram. S, D, R, and B refer to spheres, disks, rods and blades. Curved lines represent values of Corey shape factor.
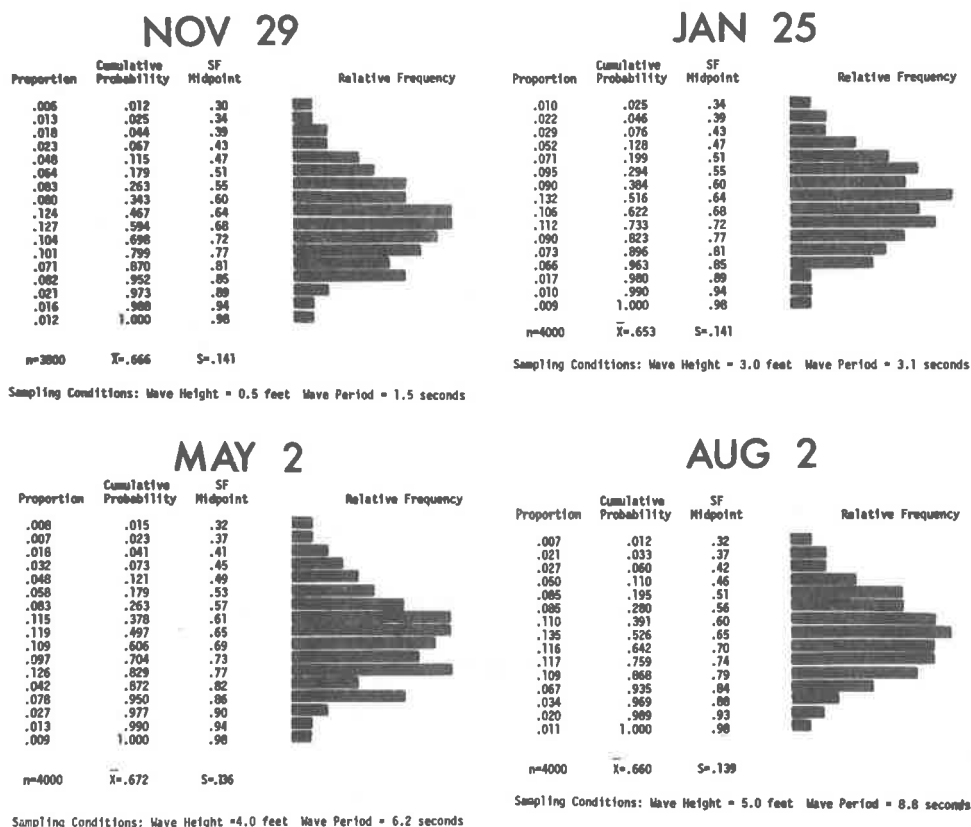
Figure 3. Distribution of Corey shape factors for the nearshore zone.

Additional data on the distribution of Corey shape factors in the nearshore zone were taken from Harrison and Alamo-Moreles (1964), who made two hundred measurements of sand grains from Virginia Beach, Virginia. These authors assumed that the sand was naturally worn quartz (Table 1). In order to provide a comparison with fluvial sands, further shape factor data were obtained from the report of Schulz et al. (1954). Of the several hundred particles measured for that study only 170 meet the qualifications of being sand size and in the range of densities 2.64 - 2.66.

DISCUSSION

Figure 3 shows the distribution of Corey shape factors for the Destin, Florida, nearshore zone. The shape factors range from 0.3 to approximately 1.0. The population statistics are summarized in Table 1. The fluvial sand grains have a mean of 0.662 which is strikingly

Table 1. Summary Statistics for Corey Shape Factors of Fluvial and
Marine Sands.

Fluvial and Marine Sands	Total Number	Mean SF	Standard Deviation
Marine Sands:			
Destin, Florida	15,800	0.663	0.140
Virginia Beach, Va.	200	0.652	0.139
		$\overline{X}=0.657$	S=0.139
River Sands (Midcontinent)	170	$\overline{X}=0.662$	S=0.138

close to the value of 0.657 for the marine samples. The range of shape
factors for the fluvial samples is between 0.5 and 0.9. The nearshore
samples are generally symmetrically distributed about their mean value.
    The difference between the measured and assumed mean value
of shape factor results in a potential 5 percent error in the estimate of
nominal size. Future use of rapid sediment or granularmetric analysis
should take this error into consideration.
    The subdivision into populations of Zingg forms shows that
spheres represent 48 percent of the population and disks, blades, and
rods represent 22, 5, and 25 percent respectively.   Comparison with
corresponding Corey shape factors indicate that the samples have a
mean SF value of 0.5 for blades, 0.7 for rods, 0.6 for disks and 0.8
for spheres. The statistics for the populations are summarized in
Table 2 and Figure 4. The subdivision based on Zingg forms does not
produce distributions that are readily amenable to statistical evaluation.
This is particularly true of the distribution of spheres. Smalley (1966)
pointed out that many shapes included in spheres are far from spherical
because of the fixed 2/3 axial ratio included in the Zingg classification.
Smalley indicated that the expected percentages for spheres are 11.1,
for blades 22.2, and disks and rods together 66.7 based upon the pro-
bability of random spatial configurations in each class. He concluded
that particle shapes are not formed at random. The distribution of
Zingg forms are presented here for the purposes of possible future
computer simulations similar to those suggested by Jizba (1966) and
Poche' (1972).
    Differences in pebble sphericity of fluvial and nearshore marine
environments have been indicated by Dobkins and Folk (1970) using the
maximum projection sphericity $(c^2(ab)^{-1/3})$ of Folk (1955). A line of
separation between the two environments was found to be at sphericities
of 0.66 (=0.54 Corey SF). Quartz pebbles from Gulf and Atlantic
coasts and rivers were used for this study. Briggs et al. (1962, in

33

Table 2. Summary Statistics for Corey Shape Factors for Zingg Groups.

Zingg Groups	Total Number	Mean SF	Standard Deviation
Spheres	7,760	0.759	0.091
Rods	3,991	0.649	0.079
Disks	3,430	0.514	0.086
Blades	799	0.438	0.080

SPHERES

Proportion	Cumulative Probability	SF Midpoint	Relative Frequency
.004	.004	.57	
.005	.008	.58	
.021	.030	.60	
.044	.074	.61	
.084	.159	.64	
.014	.173	.66	
.053	.225	.67	
.031	.257	.69	
.100	.356	.70	
.021	.378	.72	
.066	.444	.73	
.027	.472	.75	
.103	.575	.76	
.042	.617	.78	
.087	.704	.80	
.019	.723	.81	
.029	.753	.83	
.052	.804	.84	
.052	.857	.86	
.051	.908	.87	
.031	.921	.89	
.015	.936	.90	
.021	.956	.92	
.011	.967	.93	
.011	.978	.95	
.015	.994	.98	
.006	1.000	.99	

n=7660   X̄=.759   S=.091

RODS

Proportion	Cumulative Probability	SF Midpoint	Relative Frequency
.028	.035	.49	
.068	.104	.53	
.110	.214	.56	
.102	.316	.59	
.132	.448	.62	
.087	.535	.65	
.172	.707	.68	
.090	.797	.71	
.134	.931	.74	
.035	.966	.77	
.034	1.000	.80	

n=3911   X̄=.649   S=.079

DISKS

Proportion	Cumulative Probability	SF Midpoint	Relative Frequency
.010	.025	.30	
.015	.040	.32	
.024	.064	.35	
.015	.079	.38	
.050	.129	.40	
.067	.196	.43	
.091	.287	.46	
.059	.346	.48	
.127	.473	.51	
.159	.632	.54	
.126	.758	.57	
.123	.881	.59	
.081	.963	.62	
.037	1.000	.65	

n=3430   X̄=.514   S=.086

BLADES

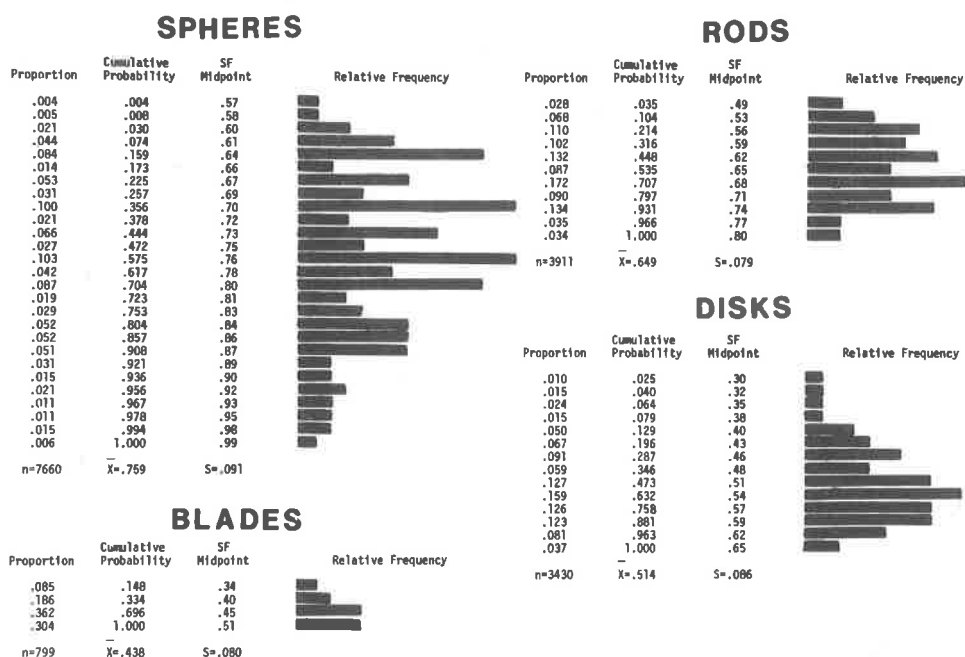| Proportion	Cumulative Probability	SF Midpoint	Relative Frequency
.085	.148	.34	
.186	.334	.40	
.362	.696	.45	
.304	1.000	.51	

n=799   X̄=.438   S=.080

Figure 4. Distribution of Zingg populations of measured grains.

errata) has indicated that the Corey shape factor correlates ($\rho = 0.997$) with the Folk maximum projection sphericity. This means that both measures are highly correlative and are both presumably valid indices of particle shape.

In the present study, no line of separation appears to exist between the sands of the fluviatile and nearshore environments. Thus, there appears to be no difference between the surf abrasive history experienced by sand grains and the fluvial abrasive history experienced by river sands. This may indicate that the shapes seen in the nearshore zone are relict and that grain shape, at least for sand, does not appear to be a valid paleo-environmental discriminator.

CONCLUSIONS

Shape study of several thousand sand grains indicates that the Corey shape factor for grains of the nearshore zone is symetrically distributed about a mean of 0.66. This is lower than the previously assumed value of 0.70 which is commonly used for rapid sediment or granularmetric analysis.

Subdivision into populations of Zingg forms shows that the most predominate shape is the sphere (48 percent). This is followed by rods (25 percent), disks (22 percent) and blades (5 percent).

There is no significant difference between the shapes of sands of fluvial environments and nearshore marine environments, as found for pebbles. This implies that there is no difference in the abrasional history between the two environments and that the shape of nearshore sands are relict.

REFERENCES CITED

Brezina, J., 1969, Granulometer - a sediment analyzer directly writing grain size distribution curves: Jour. Sed. Petrology, v. 39, p. 1627-1631.

Briggs, L. I., McCulloch, D. S., and Mosher, F., 1962, Hydraulic shape of sand particles: Jour. Sed. Petrology, v. 32, p. 645-656.

Corey, A. T., 1949, Influence of shape of the fall velocity or sand grains: unpublished M. S. thesis, Colorado State University, 102 p.

Dobkins, J. E. and Folk, R. L., 1970, Shape development on Tahiti-Nui: Jour. Sed. Petrology, v. 40, p. 1167-1203.

Folk, R. L., 1955, Student operator error in determination of roundness, spericity, and grain size: Jour. Sed. Petrology, v. 25, p. 297-301.

Gorsline, D. S., 1963, Beach studies in west Florida, U. S. A., IN Deltaic and shallow marine deposits: (Van Straaten, L. M., ed.) in Developments in Sedimentology, v. 1, p. 144-147.

_____, 1966, Dynamic characteristics of west Florida Gulf coast beaches: Marine Geol., v. 4, p. 187-206.

Harrison, W. and Alamo-Moreles, R., 1964, Dynamic properties or immersed sand Virginia Beach, Virginia: CERC Tech Memo 9, 52 p.

Inter-Agency Committee on Water Resources, 1957, Measurement and analysis of sediment loads in streams: Some fundamentals of particle size analysis: Washington, D. C., U. S. Gov't. Printing Office, 55 p.

Jizba, Z. V., 1966, Sand evolution simulation: Jour. Geology, v. 74, p. 734-743.

McNown, J. S. and Malaika, J., 1950, Effects of particle shape on settling velocity at low Reynolds numbers: Trans. A. G. U., v. 31, p. 74-82.

Poche', D. J., 1972, An estimate of sediment sieving time from computer simulation: Jour. Sed. Petrology, (in press).

Schlee, J., 1966, Modified Woods Hole rapid sediment analyzer: Jour. Sed. Petrology, v. 36, p. 403-413.

Schulz, E. F., Wilde, R. H., and Albertson, M. L., 1954, Influence of shape on the fall velocity of sedimentary particles: Omaha, Nebr., U. S. Army Corps of Engineers, Missouri River Div., Sed. Series, Report No. 5, 161 p.

Smalley, I. J., 1966, Expected shapes of blocks and grains: Jour. Sed. Petrology, v. 36, p. 626-629.

Tanner, W. F., 1960, Florida Coastal classification: Gulf Coast Assoc. Geol. Socs., Trans., v. 10, p. 259-266.

Zingg, T. H., 1935, Beitrag zur schotteranalyse: Schweiz Min. u. Pet. Mitt., Bd. 15, p. 39-140.

GENETIC AND AGE PROBLEMS OF THE MOREAU-CAMINADA

HOLOCENE COASTAL RIDGE COMPLEX,

SOUTHEASTERN LOUISIANA

By

Ervin G. Otvos, Jr.
Gulf Coast Research Laboratory
Ocean Springs, Mississippi 39564

ABSTRACT

The subrecent Moreau-Caminada ridge system in southern Lafourche Parish has formed as a prograding littoral ridge complex and not partially from river distributary mouth bars, as alleged by Ritchie (1972). No problems exist in reconciling the radiocarbon dates of the syngenetic, autochthonous peat layers in the ridges with certain dates published for the generalized positions of a number of Late Holocene Mississippi River subdeltas. Morphological considerations of the ridge system and of the southwestern part of neighboring Grand Isle suggest a possible genetic relationship between the two areas. Although there are some indications that the Moreau-Caminada ridge complex may include chenier ridges and no evidence exists to the contrary, only extensive core drilling in the swale areas could prove or disprove their presence unequivocally.

INTRODUCTION

The question of the genetic conditions and age of the Moreau-Caminada beach ridge system of southeastern Louisiana has recently reemerged in an article by W. Ritchie (1972). Earlier, the present writer has found (Otvos, 1969) that the complex developed sometime between 3000-800 yrs. B. P. through the erosion of nearby Mississippi subdeltas. Ritchie, (as Fisk; 1960), assumed that the complex started only shortly before 700 yrs. B. P. at the terminus of an active Bayou Lafourche subdelta. In Ritchie's view, it began as a series of distributary mouth bar "ridges" by the local reworking of sediments "to either side of the prograding distributary lobe" (p. 120). Subsequent additions came through the littoral drift. As Ritchie's major conclusions appear to be inadequately substantiated, his arguments must be reviewed and evaluated in the light of presently available information.

RELATIONSHIP TO MISSISSIPPI SUBDELTAS

AND THE AGE PROBLEM

Ritchie has subdivided the complex into four area units. The truncated interface between the oldest, northwestern portion and the rest of the complex, named "System 1" and "Systems 2-4" by Ritchie, has already been illustrated (Otvos, 1969, Figure 1). There is little or no real justification for separate "Systems 2-4". Neither is there any sedimentological evidence offered or available, indicating a "basic formative and physiographic difference" (Ritchie, 1972, p. 121) between "System 1" (the alleged "distributary mouth bar ridges") and "Systems 2-4". On the contrary, the very well sorted, silt-free, horizontally laminated and persistent, very fine sand layers did exhibit none of the textural and structural features typical of such bars. Moreover, distributary mouth bars are completely different, gently sloping, under-water features, whereas the northwestern Moreau-Caminada ridges even after considerable compactional subsidence, reach over 1 m above sea level. A further complication is that the term "distributary mouth beach ridges" (?) was also used in the paper (p. 121) for the same "System 1" ridges.

To accommodate the theory of the distributary mouth bar origin of the northwestern ridges and to comply with Kolb and Van Lopik's (1966) dating of the active phase of a generalized "Lafourche Delta" (1800-700 yrs. B. P.), as well as with Frazier's (1967) different and much more detailed radio-carbon dates, Ritchie found it "difficult to reconcile" my dates with the "age and distribution of delta lobes as given" by the previous three authors. As the result, Ritchie pushed aside the evidence of the three internally consistent radiocarbon dates from the maximum 3 cm thick authochthonous peat layers in two separate sand pits along La. Highway 1. Part of Ritchie's problem is his acceptance of published subdelta lobe positions as the exact locations of the ancient deltas and not as general approximations. The locations of Frazier's nearest radiocarbon-dated samples from Lobes 6 (3500-2050 yrs. B. P.) and 7 (3400-2000 yrs. B. P.), for instance, are about 40 and 60 kms, respectively, from the Moreau-Caminada complex (Frazier, 1967, p. 312-313). The exact limits of the second Lafourche Delta (Lobe 10; 2000-1200 yrs. B. P.) are equally uncertain. Although the most recent Lafourche Subdelta (Lobe 15; 250 yrs. B. P. -recent) has

obviously intruded over the western margin of the ridge complex via the Bayou Moreau distributary and must have flooded sediments into the low-lying areas, alluvium from the active deltas certainly never covered the higher ridges. This, is not contradicted by the fact that Frazier's map (p. 307) shows Lobe 15 superimposed over the subject area.

Russell (1953), tentatively supported by Shepard and Wanless (1971), earlier maintained that a generalized "Lafourche Delta" originally extended 30 miles (48 km) farther seaward and was eroded back to the present northern margin of the ridge complex. The view of Shepard and Wanless (1971, p. 213) that the "Lafourche Delta seems to be sharply truncated by the ridges", as far as the last Lafourche Lobe is concerned, is diametrically contradicted by photographic evidence.

Ritchie (p. 123) found it also difficult to accommodate my ridge complex dates with a younger radiocarbon date from Grand Isle, northeast of the Complex. Before the extensive recent erosion, the ridge complex has certainly also occupied part of the presently water-covered area, immediately northeast-east of its present limits. At one time, in my view, it may have extended over all of the waterway between Caminada Bay and the Gulf (Figure 1). The SE shore of Cheniere Caminada, defined by the youngest ridges of the Complex, and the opposite NW shore of southern Grand Isle are almost parallel to each other, as well as to the direction of the inland ridges (Conatser, 1971, p. 3052, Figure 3) of southwestern Grand Isle. In addition, the sand isopach lines of the "A" sand, which directly underlies Grand Isle (Conatser, 1971, Figure 17), also run parallel with this direction. Southwestern Grand Isle may well have been the most recent and easterly segment in the original ridge complex. The processes that somewhat later opened up the waterway between Caminada Bay and the Gulf of Mexico, eroded through an area of least resistance, probably bounded by the ridges along the present shores. This eroded area originally may have had wider swales and lower ridges than the rest of the Complex. An alternate possibility is that Sand "A" and the interior surface ridges of southwestern Grand Isle formed along the previous eastern margin of the Complex by the southwesterly littoral drift from the already eroding ridge complex after its outbuilding stopped and the drift direction reversal occurred. Despite the presently different orientations of Grand Isle and the Moreau-Caminada ridge system, the island's genetic ties with the Complex are very plausible.

One should be most hesitant about correlating soil thinness and the "morphological freshness" of the ridges with their relative youth, as Ritchie did (p. 123) in deciding whether a ridge system is 2000 or 500 years old. Factors other than a minor age difference are decisive. Certain Hancock County beach-dune ridges in SW Mississippi, which are over 2900 years old (Otvos, in prep.), for instance, have also high relief, relatively steep slopes and generally quite sparse soil cover.
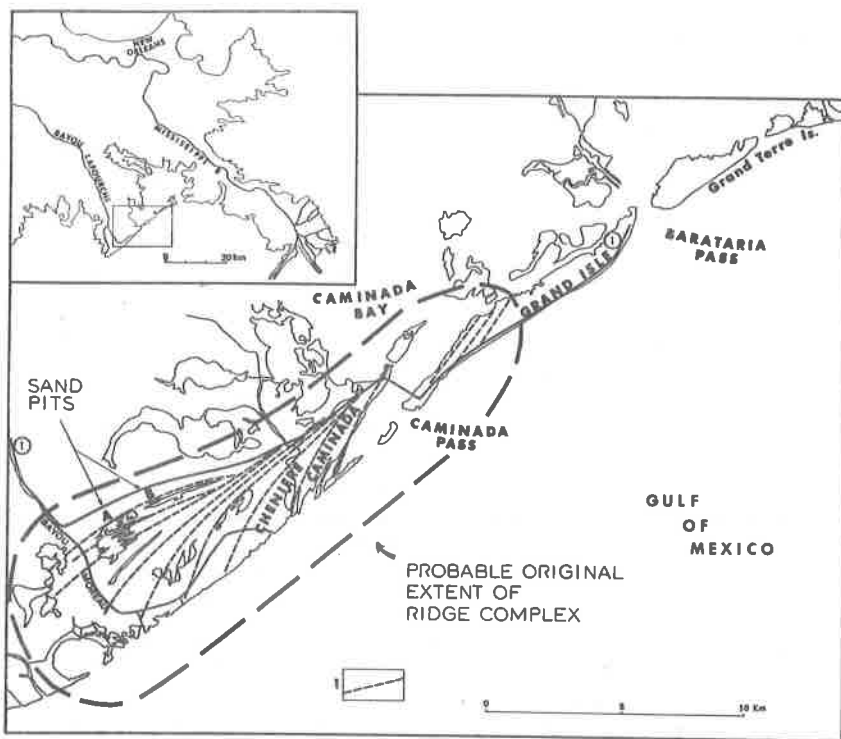
Figure 1. The Moreau-Caminada ridge complex and Grand Isle, south-
eastern Louisiana. 1-littoral ridges

BEACH BARRIER (STRAND) PLAIN OR CHENIER PLAIN?

The genetic classification of the ridge complex is an interesting
issue. The reasons cited by Ritchie against the acceptance of a chenier
origin (p. 113); "smaller size, greater ridge density, variation of alti-
tude both seaward and landward" are superficial and carry little weight.
Neither does a reference to Fisk (1955, p. 389), regarding the "absence
of marsh and bay silts at shallow depth beneath the ridge sequence".
Such deposits need not be absolute criteria for chenier origins, although
a "mixture of clay and shells" was found under the ridge sands in the
Louisiana Construction and Materials Company sand pit along Highway
1 (Galliano, personal communication, 1968). In two holes, drilled by
the Louisiana Highway Department (June 21/22, 1967) on one of the pit
sites, silty, sandy clay and silty clayey sand was found under the pene-
trated sand sequence at 8.4-9.0 m depth. In one of these drill holes at
least three clayey units were penetrated within the clean sand sequence
between 5.4-8.4 m depths.

Some view chenier plains as predominantly clay plains with
scattered sand ridges. The inter-ridge muddy sediment zones, in this
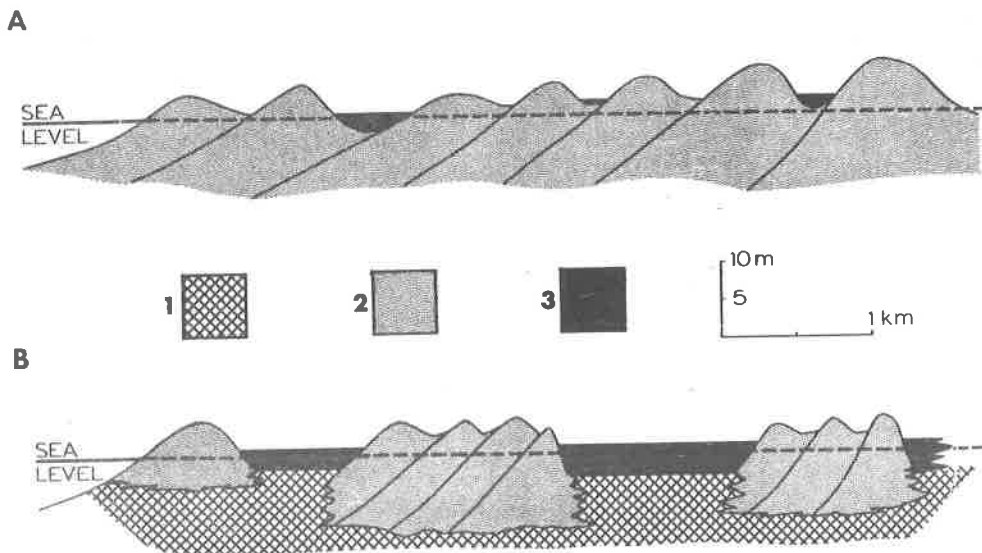
40

A

B

Figure 2. Generalized beach barrier plain (A) and chenier plain (B)
cross sections. Modified from Curray, J. R. and Moore, D.
G., 1964; and Gould, H. R. and McFarlan, E., Jr., 1959). 1-
muddy nearshore, bay, marsh-mudflat deposits; 2-shallow sub-
tidal, intertidal and supratidal sands; 3-post-ridge marsh,
swamp and alluvial deposits. Vertical and horizontal scales
flexible.

view, must be of significant widths to merit the term "chenier plain."
In my opinion quite narrow interspersed penecontemporaneous muddy
sediment belts in predominantly sand ridge - progradational sequences
should also qualify the features for the "chenier" designation, as these
belts would mark significant, if brief departures from the general sedi-
mentation pattern (Figure 2).

In the absence of adequate subsurface evidence for the origin of
the ridge complex, the interlayered peat and clay units in the sand se-
quence of the pits and the drill holes were taken as evidence that during
the early stages of ridge development the depositing sands were in later-
al contact with contemporary marsh, mudflat and/or shallow nearshore
deposits (Otvos, 1969, p. 2354). Although it is obvious that over 80-90
percent of the present Moreau-Caminada Complex area is underlain by
sand ridges, the possibility remains that sets of narrow, exclusively
sandy ridges are separated by very narrow zones of silty-clayey semi-
contemporary marsh, mudflat and near-shore deposits, which also
formed during the progradation of the Complex. Such a ridge density
is comparable with that of the Creole and Oak Grove chenier ridges,
immediately SSE of Calcasieu Lake, and of the chenier ridges between
Smith Ridge and the present beach, SE of Sabin Lake, southwestern
Louisiana.

CONCLUSIONS

No new evidence yet has been presented to refute the 3000-2000 (-800?) yrs. B. P. age of the Moreau-Caminada beach ridge system. This time range is compatible with presently available information about the locations and with the known ages of Late Holocene Mississippi subdeltas in the general area. The littoral nature of all the ridges is not in doubt but in order to clarify the "beach barrier plain" or "chenier plain" origin of the Complex, a line of coreholes should be drilled at right angle to the direction of the ridge axes. Only this could confirm that the observed intercalated clayey, silty and peaty units are not localized within the ridge sets but are indeed also related to narrow progradational muddy inter-ridge sediment belts.

REFERENCES CITED

Conatser, W. E., 1971, Grand Isle: a barrier island in the Gulf of Mexico: Geol. Soc. of Amer. Bull., v. 82, p. 3049-3068.

Curray, J. R. and Moore, D. G., 1964, Holocene regressive littoral sand, Costa de Nayarit, Mexico, in Developments in Sedimentology, v. 1, Deltaic and shallow marine deposits: Elsevier Publ. Co., Amsterdam, p. 76-82.

Fisk, H. N., 1955, Sand facies of recent Mississippi Delta deposits: Proc. 4th World Petrol. Congress, Rome, v. 1, p. 377-397.

_____, 1960, Recent Mississippi River sedimentation and peat accumulation: Compte Rendu quatrième Congres pour l'avancement études stratigraphie et géol. du carbonifère, p. 187-199: Heerlen.

Frazier, D. E., 1967, Recent deltaic deposits of the Mississippi River: their development and chronology: Trans. Gulf Coast Assoc. of Geol. Soc., v. 17, p. 287-315.

Gould, H. R. and McFarlan, E., Jr., 1959, Geologic history of the chenier plain, southwestern Louisiana: Trans. Gulf Coast Assoc. of Geol. Soc., v. 9, p. 261-270.

Kolb, C. R., and Van Lopik, J. R., 1966, Depositional environments of the Mississippi River delta plain-Southeastern Louisiana, in Deltas and their geological framework: Houston Geol. Soc., p. 17-61.

Otvos, E. G., Jr., 1969, A subrecent beach ridge complex in Southeastern Louisiana: Geol. Soc. of Amer. Bull., v. 80, p. 2353-2358.

_____, In preparation, A Late Holocene beach ridge system ("Hancock County Chenier"), southwestern Mississippi Coast.

Ritchie, Wm., 1972, A preliminary study of the distribution and morphology of the Caminada/Moreau sand ridges: Southeastern Geol., v. 14, p. 113-125.

Russell, R. J., 1953, Coastal advance and retreat in Louisiana: Congress Geol. Intl., 19th Sess., Comptes Rendus, v. 40, no. 12, p. 108-118.

Shepard, F. P. and Wanless, H. R., 1971, Our changing coastlines: McGraw Hill Publ. Co., 579 p.

BEACH RIDGE SLOPE ANGLES vs AGE

By

William F. Tanner
and
John C. Hockett
Geology Department
Florida State University
Tallahassee, Florida

ABSTRACT

Sixteen beach ridge sets, including 76 Holocene beach ridges, have been studied in the field in northwest Florida. Beach ridge side slope and age were determined, along with other data. Five important data points emerged, at about 200, 200, 400, 3,500 and 5,000 years ago. All ridge sets at any one age have the same side slopes (excluding dune decoration); older ridges have gentler side slopes. The available data points, when plotted on semilog paper, fix a line close to:

$$Ln\ t = 12.37 - i$$

(i = surface slope; t in years). Older ridges, providing many slope measurements, fall on this line at about 120,000 years ago (Sangamon time). No ridges, on sand of the same size and under the same climate, would be visible after about 170,000 years. This line provides a method of estimating ridge age in certain selected areas where materials are not too coarse.

INTRODUCTION

A beach ridge is a linear depositional body having a long more-or-less straight (or gently curving) crest line, and two sloping sides. A long, narrow, straight roof, slanting gently downward in opposite directions from the peak, makes a reasonably good model for visualization purposes.

At any representative spot on one of the sloping sides, the surface is composed of loose particles, typically but not necessarily sand. Sand grains on or near this surface are moved rather easily by various agencies: rain splash, animal feet, boring or tunneling organisms, plant shoots, wind. In a statistical sense, any one grain is likely to come to rest, after being disturbed, at a new position farther down the slope than it had occupied shortly before. The actual details of transport are much too complicated to present in an analytical expression, but the general history of the slope can be approximated easily.

Loose grains on steep slopes are more likely to be moved than loose grains on gentle slopes, and this motion is more likely to have a unidirectional (down-slope) bias. Transport of this kind will tend, in due time, to lower the slope angle, which in turn reduces the probability that further transport will take place. That is, the apparently random disturbing influences, cited above, provide that the slope will get gentler as time passes.

This general approximation can be stated as

$$\frac{di}{dt} = \frac{-k}{t} \tag{1}$$

where i is the slope angle, t is time in years, and k is a numerical co-efficient which will be estimated or determined later. Eq. (1) says that the rate of change of the slope angle is inversely proportional to the length of past history of the slope: young, steep slopes (of the kind specified here) change more rapidly than old, gentle slopes. The minus sign says that the slope is growing gentler as time passes. Eq. (1) integrates directly to

$$i = -k \ln t + c \tag{2}$$

where c is a constant of integration which remains to be specified.

The thinking reviewed above leads to the suggestion that beach ridge slopes, from ridges of different ages, be measured in the field in an effort to supply data from which estimates of k and c can be made. Accordingly a field program was undertaken, along the coast of northwest Florida, where a great deal of other study has provided information about the histories of several beach ridge plains.

FIELD DATA

Eighteen sets of beach ridges were selected for field work: one set on Dog Island, two sets on St. George Island, two sets on St. Vincent Island, two sets on Alligator Peninsula, and eleven sets on the Mainland in the strip where the towns of Panacea, Carrabelle and Apalachicola are located (Figure 1). The number of slopes measured was 373; the average mainland set contained 25 slopes, and the average for the other sets was 13.5 slopes. Each slope was measured in the field with the clinometer device which is part of a Brunton pocket transit.

All of the mainland sets fell into the same population ("population 1"), having a mean value of $0^{\circ}42'$ and a standard deviation of $0^{\circ}05'$ (the maximum angle obtained in these 11 sets was $1^{\circ}05'$). As is suggested by the small standard deviation, any one of these sets can be taken to represent all 11 of them. Furthermore, no other set had a mean slope as small as 2°. Hence, the mainland beach ridges fit into a distinctive population of very subtle features, quite unlike those on the offshore islands. This distinction is immediately obvious on the ground, and also on air photos of the area.

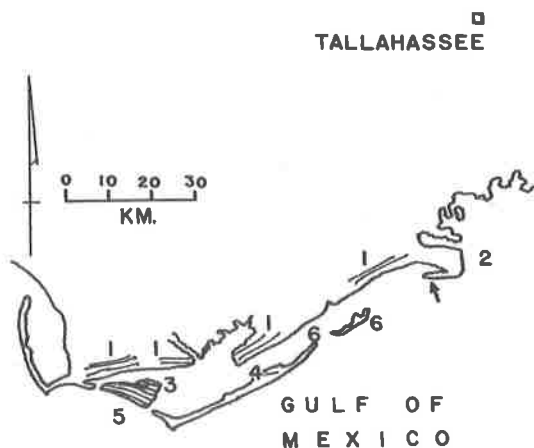The age of "population 1" is not known, except that it must be

TALLAHASSEE

Figure 1. Outline map of the study area, south-
west of Tallahassee, Fla., showing the loca-
tions of various beach ridge sets. Ridges
marked as Population No. 1 are on the main-
land and are clearly the oldest in the area.
Population No. 2, on a headland, is character-
ized by hummocky topography and erratic
side slope angles; these data were not used.
Populations 3, 4, 5 and 6--located on islands
-- are of Holocene age, but were not formed
simultaneously. All of the Population No. 1
sets have the same side slope angle. Popula-
tion 6-A (to the west) and 6-B (to the east) dif-
fered slightly from each other in side slope
angles. The arrow marks the location of an
additional set, not used here, because of un-
certainty in the age.

significantly older than about 30,000 years (carbon-14 data from much
younger materials).

The remaining sets produced means varying from a low of $2°08'$
(standard deviation of $0°16'$) (population 2") to a high of $7°38'$ (standard
deviation of $0°22'$) ("population 6"). "Population 3", for example, had
a mean slope of $4°00'$ (standard deviation $0°43'$), and hence is distinct
from "population 2." The means for the first three populations (1, 2,
3) are, depending on the starting mean, 5.4, 7.0, 17, or 2.6 standard
deviations apart, hence, these populations can be taken as distinct
from each other.

In a rather general way, the steeper slope sets have larger
standard deviations, but only one was larger than $0°24'$.

The younger ridge sets (populations 3, 4, 5 and 6) are found

47

largely on offshore islands, where a reasonably detailed history is known, or can be inferred, from air photos spread over a 35 year period, charts and maps over 130 years, records, kitchen middens, and carbon-14 ages. Dates obtained from this information are not precise, but are strictly limited estimates.

LABORATORY DATA

The sand size for each locality was obtained by sieving (quarter-phi screens, 30 minutes sieving time). None of the grain size data sets could be distinguished from the others, on the basis of means and standard deviations. Hence, it was concluded that the beach ridge sand size was essentially the same (2.076 Φ) throughout the study area, as far as the requirements of the present investigation are concerned. Digestion of carbonate, in HCl, was undertaken for a representative sample from each set, but the mean size was not changed significantly in any sample. This last finding is consonant with the general understanding that, in the study area, carbonate is largely lost to leaching in the first decades or few centuries.

One additional check was undertaken: a study of the angle of repose of samples from each area, both dry and wet. For all dry sand samples, the average angle of repose was 38.5° (standard deviation 0.132°), and for sand under water, the average angle of repose was 34.55° (standard deviation 0.024°). All of the areas contain sand that comes to rest at the same angle of repose; furthermore, this angle does not seem to be pertinent, being five times as great as the steepest observed beach ridge slope.

REGRESSION LINES

The data for populations "3" through "6" were plotted on semi-log paper, with time shown on the log ordinate (Figure 2). Five known points were obtained in this fashion, at dates close to 200 years, 200 years, 400 years, 3,500 years and 5,000 years ago.

The side slope angles have been plotted as mean values, and the standard deviations show that various sets can be distinguished from each other. The ages, however, are less precise: they are limited by historical, archeological, and C-14 dates, but there are no mean values between these limits. For this reason, calculation of regression lines is probably not much improvement, if any, over free-hand sketching of a "correlation" line. Nevertheless, four precise age estimates were made for each population, and these various estimates were used in computing four regression lines (Figure 2). The latter were then combined, with equal weights, to produce a "best estimate" line as follows:

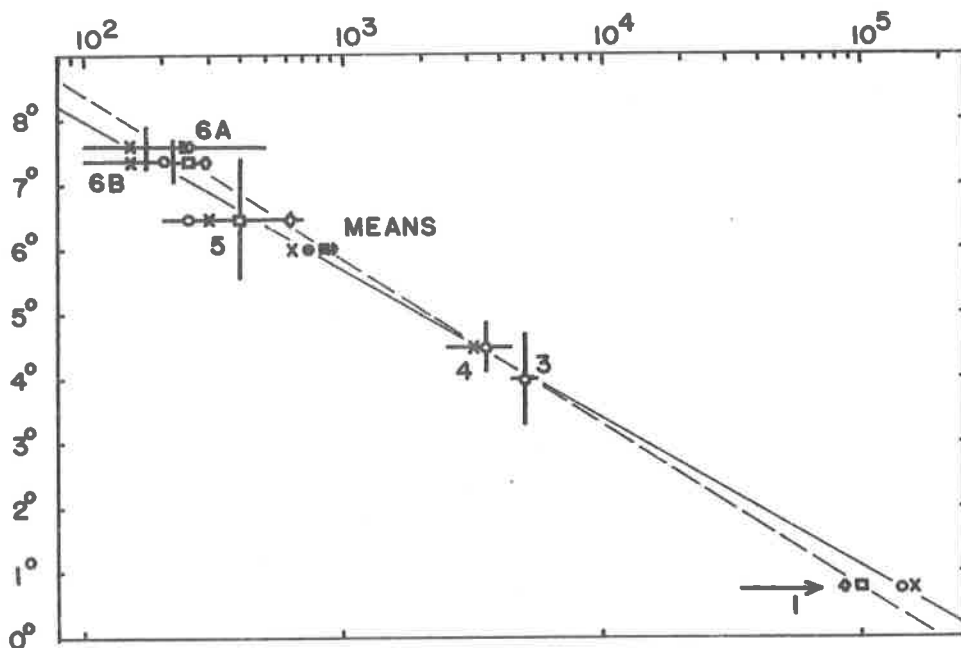$$\text{Ln } t = 12.37 - i \qquad (3)$$

Figure 2. Beach ridge side slope (in degrees) vs. age (in years). The
chart is based on five data points (Numbers 3, 4, 5, 6-A and
6-B). Side slope measurements are represented by precisely
calculated mean values, with an associated vertical bar showing
one standard deviation above, and one standard deviation below,
the mean. Ages are limited by historical records, kitchen
midden debris, and C-14 dates; in this kind of dating, averages
are not known, but maximum and minimum values are shown by
the horizontal bar given for each slope mean. The information
available for Population No. 3 provides a rather closely control-
led age (short horizontal bar). Populations 5, 6-A and 6-B, al-
though much younger, are not as easy to define on a log-time
scale. Because of the time uncertainties, only representative
ages (or dates) can be used. Four such selections have been
made, shown by the following symbols (except where full plotting
produced too much crowding): x, open circle, open box, open
diamond. Four regression lines were calculated, one for each
set of ages. The four means are shown (solid black symbols).
Obviously other choices could have been made for ages, and the
results would have varied accordingly. Two of the regression
lines have been drawn. Population No. 1, of unknown age but
clearly pre-Holocene, has been located on the four regression
lines, by the appropriate symbols (lower right corner), thereby
producing an estimate of the age: somewhere between about
85,000 years B. P. and 160,000 years B. P. An average of
these four ages is close to 120,000 years B. P. A free-hand
"correlation" line, fitted according to our best interpretation of
the information, produced a date for No. 1 at about 100,000 -
110,000 years B. P.

where t is age in years, and i is slope angle in degrees.

"Population 2" data, although collected in the field early in the course of the work, were finally rejected, specifically because as familiarity with other beach ridge sets increased, it became evident that "population 2" ridges had been decorated with small hummocks of eolian sand, and perhaps in other ways, giving erratic and locally steep results.

"Population 1" Slope data--the oldest-were placed on the correlation lines where they intersected the average slope angle ($0^{\circ}42'$). The lines then provided an estimated age for "population 1" ridges: somewhere between 85,000 and 160,000 years old, with an "average" value of about 120,000 years.

Although there are uncertainties concerning the precise values for some of the ages (note, however, that the date for population No. 3 is severely limited), the conclusions to be drawn from eq. (3) cannot be modified very much. For example, it is not possible to combine the data so as to make population No. 1 less than 70,000 years old, nor is it possible to make population No. 1 as much as 250,000 years old.

Projection of the lines provides that no slopes would exist, on this sand and under this climate, after roughly 200,000 years. In fact, if $0^{\circ}20'$ is the lower limit of field visibility of a beach ridge side slope, no ridges would be seen after 150,000 to 220,000 years.

DISCUSSION

Hundreds of ionium disequilibrium dates (Osmond, May and Tanner, 1970; and later results) and many carbon-14 dates, as well as historical reference points, have been obtained in the course of coastal studies at Florida State University. It is current practice here to identify a high MSL position, about 110,000 years ago, as being of Sangamon (interglacial) age. It has been our observation that, except for erratic items of dubious value, and questionable C-14 dates, all dates of clearly defined coastal depositional features (observed in various parts of the Americas and particularly around the Gulf of Mexico) fall into either Sangamon and earliest Wisconsin, or late Holocene, time. Hence, the inferred age for the pre-Holocene ridges (population No. 1) is in agreement with the radiometric ages of the youngest large pre-Holocene coastal deposits in the same region.

In the study area, sharply-defined beach ridges are no older than late Holocene, and poorly-defined beach ridges are about Sangamon in age. It is not now clear how far afield one might extrapolate these observations. It seems obvious that they will not apply to ridges made of gravel, hence eq. (1) should be modified to:

$$\frac{di}{dt} = \frac{-k\ fn\ (g)}{t} \qquad (4)$$

where g is a measure of grain size, but no data are at hand for evaluating fn (g).

The effects of climate differences, or changes in windiness or other possible parameters, are not so obvious. In the beach ridge plain west of the Gulf of Venezuela (Tanner, 1971), some of the steepest slopes are slip faces on eolian accumulations on top of the oldest beach ridges. However, anomalies of this kind should be relatively easy to identify, and, therefore, perhaps climate restrictions will be less severe than grain size uncertainties.

Individual beach ridges typically form in intervals of markedly less than 100 years. During the time of development of one ridge, destructive agencies may alternate with constructive agencies such as the swash, but the ridge exists in a regime of growth. At some time typically much less than 100 years after its initiation, the ridge will be isolated (by a younger ridge) from swash action, and the destructive history will begin. For the present report, the destructive regime is taken to start at an age of 100 years (an estimate that is somewhat too high). Projecting the tentative lines back to 100 years gives a maximum initial side slope of about 8°. This is not a slope equivalent to that on many modern sandy beaches: the latter are not, in general, producing beach ridges.

REFERENCES

Osmond, J. K., J. P. May, and W. F. Tanner, 1970, Age of the Cape Kennedy barrier-and-lagoon complex: Jour. Geophysical Research, v. 75, p. 469-479.

Tanner, W. F., 1971, Growth rates of Venezuelan beach ridges: Sedimentary Geology, v. 6, p. 215-220.

Volume 14, Number 4, Mississippi Gulf Coast Pleistocene Beach Barriers and the Age Problem of the Atlantic-Gulf Coast "Pamlico"--"Ingleside" Beach Ridge System.

Figure 1.   Generalized location map of Ingleside-Pamlico Barrier ridges along the Gulf and Atlantic coasts.
A-Ingleside-Live Oak Chain
B-Mississippi Coast ridges (Waveland-Belle Fontaine Pt.)
C-Apalachicola Delta Coast ridges
D-Cape Kennedy ridge complex
S-buried ridges, S. E. Louisiana

(Note: With the exception of the Mississippi Coast barrier ridges and those between Destin and Fort St. Joe, Florida, studied by the author, ridge locations are based on published papers and written communications.)

Figure 2.   Mississippi Coast Barrier Beach System
Symbols: 1-Holocene alluvium, marsh and beach deposits
2-Pleistocene barrier ridges (Gulfport Formation, Sangamon interglacial)
3-Pleistocene alluvial deposits (Sangamon Prairie-Pamlico and early Wisconsin)
4-Earlier Pleistocene alluvial deposits (?="Second"/ "Irene" Terrace surface and underlying unit in SE Louisiana)
5-Pre-Pleistocene sediments. Mostly Pliocene: alluvial-fluvial Citronelle Formation. Small areas of Miocene.

Sample locations: (I) Biloxi Formation: 1-Industrial Seaway, Gulfport; wood trunks (42,000+ yrs. B. P.); 2-Lewis Avenue, Gulfport; shell fragments, (40,000+ yrs. B. P.); 3- Pass Christian, City Park, oyster shells, 18-26 feet below surface 37,000+ 1800 yrs. B. P.; originally "dead", contaminated sample); (II) Gulfport Formation: 4-Bay St. Louis; Th/U-dated Crassostrea shell (95,000 yrs. B. P.); 5-Rodenberg Ave., Biloxi; humate in beach sand (40,000+ yrs. B. P.); 6-Belle Fontaine Pt.; disseminated carbonaceous (humate) material (35,000? yrs. B. P.); (III) Prairie Formation: 7- Wolf River; Late Pleistocene peat sample (41,000+ yrs. B. P.); 8- Van Cleave Road, North of Ocean Springs; back-swamp peat, (27,000+yrs. B. P.). 9-Deer Island: NW end, south beach, intertidal, close to eroding subrecent marsh peats (16,635+255 yrs. B. P.; originally "dead", contaminated sample).